

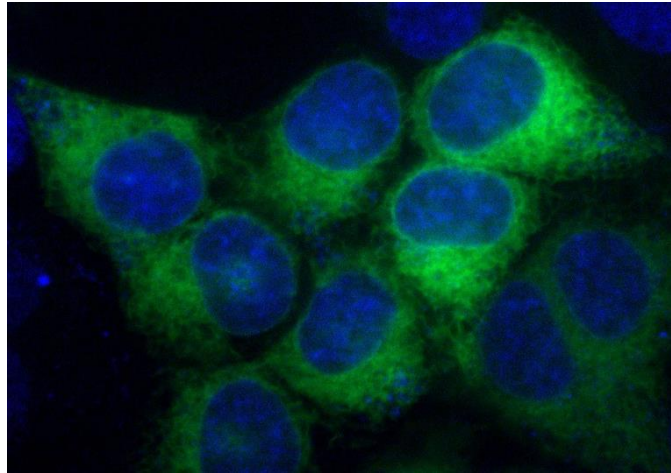


**SAPIENZA**  
UNIVERSITÀ DI ROMA

**DOTTORATO DI RICERCA IN BIOCHIMICA**

**CICLO XXIX (A.A. 2013-2016)**

**“PDIA3: a versatile and pleiotropic protein disulfide  
isomerase”**



**Docente guida**  
**Prof. Fabio Altieri**

**Coordinatore**  
**Prof. Francesco Malatesta**

**Dottoranda**  
*Ilaria Marrocco*

## CONTENTS

<b>1. INTRODUCTION</b> .....	1
<b>1.1 Thioredoxin superfamily</b> .....	1
<b>1.2 Protein Disulfide Isomerase family</b> .....	3
<b>1.3 PDIA3 protein</b> .....	5
<i>1.3.1 PDIA3 in the ER</i> .....	6
<i>1.3.2 PDIA3 in the cytosol</i> .....	7
<i>1.3.3 PDIA3 in the nucleus</i> .....	9
<i>1.3.4 PDIA3 on cell membrane and secretion</i> .....	11
<b>1.4 PDIA3 and diseases</b> .....	12
<i>1.4.1 PDIA3 and Alzheimer's disease</i> .....	13
<b>1.5 ER stress and UPR</b> .....	14
<i>1.5.1 IRE1</i> .....	16
<b>1.6 Flavonoids</b> .....	19
<b>2. AIMS OF THE RESEARCH</b> .....	22
<b>3. MATERIALS AND METHODS</b> .....	25
<b>3.1 Reagents</b> .....	25
<b>3.2 Protein expression and purification</b> .....	25
<b>3.3 Fluorescence Quenching Measurements</b> .....	26
<b>3.4 Determination of Protein Disulfide Reductase Activity</b> .....	27
<b>3.5 Determination of DNA Binding Activity by EMSA</b> .....	27
<b>3.6 Statistical analysis</b> .....	28
<b>3.7 Cell cultures</b> .....	28
<b>3.8 Cell lysate preparation</b> .....	28
<b>3.9 Proteins precipitation in culture medium</b> .....	29
<b>3.10 Western blot</b> .....	29
<b>3.11 Cell viability assay</b> .....	30
<b>3.12 Immunofluorescence</b> .....	30
<b>3.13 Mutagenesis, lentiviral production and infection</b> .....	31
<b>3.14. Knockdown of PDIA3</b> .....	32
<b>3.15 Total RNA extraction, and Reverse Transcription-PCR</b> .....	32
<b>3.16 Real-time PCR</b> .....	32
<b>3.17 XBP1 splicing assay</b> .....	33
<b>3.18 Live Cell Imaging</b> .....	34
<b>4. RESULTS AND DISCUSSIONS</b> .....	35
<b>4.1 Comparative analysis of the interaction between different flavonoids and PDIA3</b> .....	35
<i>4.1.1 Flavones eupatorin and eupatorin-5-methyl ether bind PDIA3 with high affinity</i> .....	35
<i>4.1.2 Effect of flavonoids on the PDIA3 redox activity</i> .....	41

4.1.3 Effect of flavonoids on the DNA binding property of PDIA3 .....	42
4.2 Involvement of PDIA3 in $\beta$ -amyloid deposits .....	44
4.2.1 $\beta$ -amyloid peptide treatment causes a decrease in PDIA3 protein but not in mRNA levels in SH-SY5Y cells .....	44
4.2.2 The 25-35 fragment of the amyloid $\beta$ peptide does not induce ER stress in SH-SY5Y cells .....	47
4.2.3 $\beta$ -amyloid peptide treatment does not induce an PDIA3 degradation via proteasome in SH-SY5Y cells .....	51
4.2.4 $\beta$ -amyloid peptide treatment induces PDIA3 delocalization and secretion in SH-SY5Y cells .....	52
4.3 Discriminating between IRE1 activities .....	56
4.3.1 IRE1-GFP cleaves XBP1 mRNA and clusters in foci. ....	56
4.3.2 An IRE1GFP defective luminal domain mutant is completely inactive .....	61
4.3.3 An IRE1GFP defective endoribonuclease domain mutant does not cleave XBP1 mRNA but clusters irreversibly into ER membrane.....	62
4.3.4 The flavonoid luteolin induces XBP1 splicing acting from the cytosol but does not induce IRE1 clustering.....	67
4.3.5 L827P IRE1-GFP is a fortuitous inactive mutant found in our lab. ....	70
5. CONCLUSIONS .....	76
REFERENCES.....	80



## INTRODUCTION

### 1.1. Thioredoxin superfamily

Thioredoxins (Trx) are small globular proteins that are found in all living cells from archeobacteria to humans [Holmgren, 1985]. These proteins are involved in several biological functions including dithiol hydrogen donation in ribonucleotide reduction, structural roles in coliphages such as f1 and M13, regulation of the activity of photosynthetic enzymes and some eukaryotic transcription regulation factors [Holmgren, 1989; Jacquot et al., 1994; Holmgren, 1995]. Members of this family contain an active site with the CXXC sequence, also known as the “Trx-motif”. The oxidized form of the protein is reduced by a NADPH-linked system, present in all types of the cells, in which Trx obtains electrons from NADPH via the flavin enzyme thioredoxin reductase (TrxR) [Štefanková et al., 2005].

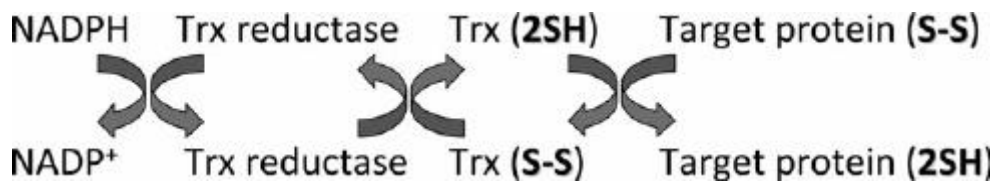


**Figure 1.** Thioredoxin NADPH-linked system schematic representation.

This system is a general disulfide reductase and catalyzes NADPH-dependent reductions of exposed S-S bridges in a variety of proteins [Holmgren, 1985]. The 3-D structures of Trx proteins are highly conserved and are characterized by a central core, consisting of five  $\beta$ -sheets surrounded by four  $\alpha$ -helices [Holmgren, 1995; Martin et al., 1995]. This structural configuration is known

as thioredoxin fold and is present in different protein families, such as protein disulfide isomerases (PDIs), in DSB (disulphide bond formation) proteins, in glutaredoxin (Grx), in the glutathione reductase and glutathione peroxidase.

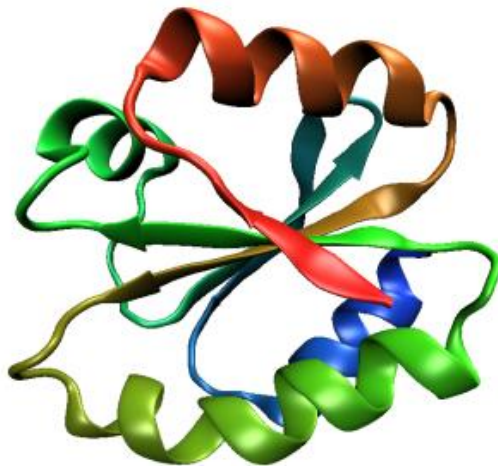


**Figure 2.** The typical Trx-fold.

The structural features that are conserved in Trx family members, such as the Trx-fold and the specific primary and secondary structures, lead to a different reactivity in catalysing protein disulfide interchange reactions. It has been shown that both active site cysteine residues play an important role in the differentiation of the properties across the family and that the relative stability (depending on cysteines nucleophilicity) of thiolates determines whether these enzymes catalyze oxidation, reduction or isomerization of thiol residues in protein substrates. Following this line, Trx is a good reducing agent because its cysteine thiolates are both poorly stabilized; DsbA is a good oxidizing agent (it stabilizes both cysteine thiolates) and isomerases like PDI have one thiolate (solvent exposed) poorly stabilized and the other (buried)

highly stabilized [Cheng et al., 2011; Hatahet et al., 2009; Carvalho et al., 2009].

## 1.2. Protein Disulfide Isomerase family

The protein disulfide isomerase (PDI) family is composed by 21 known proteins in humans that belong to the thioredoxin superfamily, classified by sequence and structural homology.

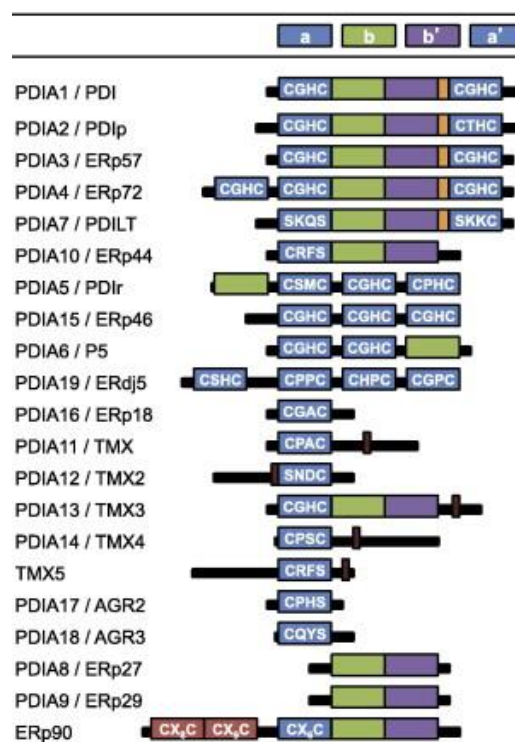


**Figure 3.** PDI family members in humans. In blue: catalytic domains *a* and *a'*, in green and purple non catalytic *b* and *b'* domains.

These enzymes catalyze the formation, reduction or isomerization of disulfide bonds of newly synthesized proteins in the lumen of the endoplasmic reticulum (ER). They are also part of a quality-control system, thanks to their molecular chaperone function. These proteins show a structural organization with multiple domains; each domain shows the typical Trx-fold and two or three of these domains contain the redox-active -CXXC- motif, while the others are considered Trx inactive domains [Turano et al., 2002]. Thanks to these redox-inactive domains, PDIs have the ability to bind peptides or proteins and to exert a molecular chaperone function [Ferrari et al., 1999; Ellgaard et al., 2005]. The number, the arrangement of tioredoxin-like domains and the specific sequence of the catalytic -CXXC- motif can be used to differentiate the members of this family. These differences determine their respective role in the oxidative folding, but also contribute to their specific functions in other pathways. Furthermore, the differences in their redox active motifs can reflect separated roles in oxidation, reduction and isomerization [Maattanen et al., 2006].

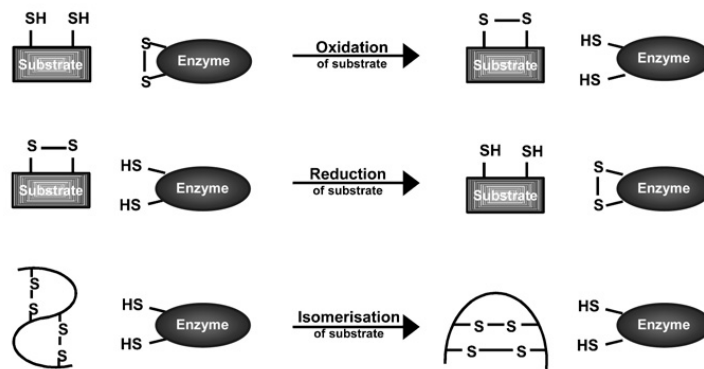


**Figure 4.** PDIs disulphide bond exchange. Depending on the redox form, they can catalyse oxidation, reduction or isomerization.

## 1.3. PDIA3 protein

PDIA3, encoded by the gene *PDIA3* on chromosome 15, is a protein of 505 amino acids and a molecular weight of 57KDa. It is also known as ERp57, ERp60 or GRp58 (glucose-related protein 58). Its structure contains four Trx-like domains: *a* and *a'* are redox active and contain the active site constituted by the tetrapeptide CGHC (cysteine-glycine-histidine-cysteine), while *b* and *b'* domains are redox inactive.

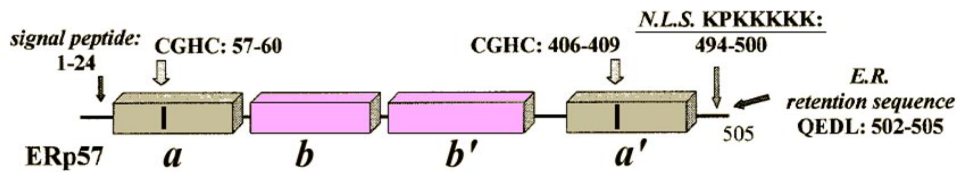


**Figure 5.** Protein PDIA3 modular structure.

PDIA3 modular structure is similar to the one of PDI, but lacks the C-terminal acidic region. At the amino acid level, similarity is highest in the catalytic domains *a* and *a'* (about 50 %) and lowest in the *bb'* domains (20%) [Kozlov et al., 2006]. The C-terminus contains a gln-glu-asp-leu (QEDL, 502QEDL505) sequence that is similar to the canonical ER-retention sequence (KDEL) and a nuclear localization signal (NLS, 494KPDKKKKK500). Deletion and mutation experiments revealed that NLS is fundamental for PDIA3 translocation in the nucleus. Furthermore, both C-terminal NLS/ER regions are required for ER retention following PDIA3 targeting to the ER through the hydrophobic N-terminal signal peptide. It has been demonstrated that an overlapping NLS/ER retention signal is required for nuclear localization and ER retention of PDIA3 [Adikesavan et al., 2008].

The canonical ER retention signal sequence is KDEL, whose binding to KDEL receptors ensures retention in the ER, for proteins normally present in the ER that have been transported beyond this compartment [Pelham et al., 1988]. It has been hypothesized that variations between retention sequences (e.g. QEDL, KEEL) may influence their cellular sorting and localization [Turano et al., 2002]. Protein disulfide isomerase PDIA3 is localized predominantly in the ER but is also present in the cytosol, in the nucleus and on the cell surface [Adikesavan et al., 2008; Jordan et al., 2006].

### ***1.3.1. PDIA3 in the ER***

PDIA3 is mainly located in the ER, where it participates to the correct folding and to the quality control of neo-synthesized glycoproteins meant to be secreted or localized to the cell membrane. To do this PDIA3 interacts with lectins calreticulin (CRT) or calnexin (CNX), which are responsible for recognizing and binding to monoglycosylated proteins [Oliver et al., 1997; Molinari et al., 1999; Oliver et al., 1999]. It has been reported that modifications of specific residues in the *b'* domain of PDIA3 reduce or abolish its binding to calreticulin, indicating that this domain is responsible for the interaction [Russell et al., 2004]. PDIA3, in complex with CRT/CNX, performs disulfide shuffling, a process that requires the intermediate formation of a mixed disulfide between the glycoprotein and the proximal cysteine of one of the two active sites of PDIA3. The shuffling is then completed by the intervention of the distal cysteine present in the same active site. A second important function of PDIA3 in the ER is the participation in the assembly of the major histocompatibility complex (MHC) class I [Lindquist et al., 1998]. An efficient antigen processing through the MHC I

requires the formation of the peptide-loading complex (PLC). This complex consists of the transporter associated with antigen processing (TAP) as centerpiece, which recruits the major histocompatibility complex class I (MHC I) heavy-chain/ $\beta$ 2-microglobulin dimer by the adapter protein tapasin (Tsn). The transient Tsn-MHC I interaction is stabilized by PDIA3, and the endoplasmic reticulum (ER) chaperone calreticulin (CRT), which recognizes the monoglucose unit of N-core glycosylated MHC I molecules. In the PLC PDIA3 interacts with tapasin [Dick et al., 2002]; the structure of this complex has been resolved at 2.6 Å resolution [Dong et al., 2009]; this was the first time in which the whole 3D structure of PDIA3 was obtained. Both a and a' domains of PDIA3 are involved in the interaction with tapasin. The cysteine 57 in the a domain of PDIA3 forms a disulfide bond with cysteine 95 of tapasin, while the a' domain-tapasin interaction is entirely non-covalent. The tapasin-PDIA3 complex is essential in the assembly and the stabilization of the PLC; PDIA3 shows a structural role rather than a catalytic one. In fact the suppression of PDIA3 affects the stability of PLC and decreases both the expression of MHC on the cell surface and the peptide loading within the PLC [Garbi et al., 2006]. PDIA3 also modulates the activity of sarco/endoplasmic reticulum calcium ATPase (SERCA), a  $\text{Ca}^{2+}$ -ATPase that transfers  $\text{Ca}^{2+}$  from the cytosol to the lumen of the ER, by regulating the redox state of the sulfhydryl groups in the intraluminal domain of SERCA [Li et al., 2004].

### ***1.3.2. PDIA3 in the cytosol***

PDIA3 has been reported in the cytosol thanks to the interaction with other proteins. In this localization it associates with STAT3 [Sehgal, 2003]. STAT3

is a member of the STAT (Signal Transducer and Activator of Transcription) family. In response to cytokines and growth factors, these proteins are phosphorylated by receptor-associated kinases and then form homo- or hetero-dimers that translocate to the cell nucleus, where they act as transcription activators. STAT3 is activated through phosphorylation of tyrosine 705, in response to various cytokines and growth factors including interferons, epidermal growth factor and interleukin-6 (IL-6). The binding of IL-6 family cytokines to gp130 receptors triggers STAT3 phosphorylation by JAK2. Hyperactivation of STAT3 is frequently observed in a variety of human cancers, including head and neck cancer [Yu et al.,2004; Yu et al, 2009; Song et al., 2000]. Continuous STAT3 activation allows the growth and survival of cancer cells through modulation of cell cycle regulators (e.g., cyclin D1/D2 and c-Myc), upregulation of anti-apoptotic proteins (e.g., Mcl-1, Bcl-xl, and survivin), downregulation of the tumor suppressor p53, and induction of angiogenesis by vascular endothelial growth factor (VEGF); these mechanisms lead to tumor progression and resistance to anti-cancer drugs [Frank, 2013; Yu et al.,2004; Yu et al, 2009]. It has been reported that PDIA3 modulates STAT3 activity [Eufemi et al., 2004; Chichiarelli et al., 2010], although there are controversial results [Coe et al., 2010]. For instance, PDIA3 has been reported to interact with and enhance STAT3 activity in melanoma and hepatoma cells [Eufemi et al., 2004; Chichiarelli et al., 2010], whereas another group suggested that this PDIA3-STAT3 complex negatively affects STAT3 DNA-binding activity [Coe et al., 2010]. Hence, the role of PDIA3 in the STAT3 activity regulation is still not completely defined.

As a further proof of PDIA3 presence in the cytosol, it was found in

association with mTOR [Ramírez-Rangel et al., 2011]. mTOR is a serine-threonine protein kinase, found in two multiprotein complexes called mTORC1 and mTORC2, which regulate cell proliferation. PDIA3 contributes to the assembly of mTORC1, activates the kinase activity of mTOR, and also participates in the mechanism by which mTORC1 detects its upstream signals, such as stimulation by insulin or nutrients. PDIA3 over-expression induces cellular proliferation, while PDIA3 knockdown opposes the proliferation induced by insulin and nutrients. It is reasonable that part of this behaviour is related to the mTOR-PDIA3 interaction, considering that mTOR is involved in the regulation of proliferation.

### *1.3.3. PDIA3 in the nucleus*

PDIA3 was found for the first time in the nuclei of 3T3 cells and rat spermatids [Ohtani et al., 1993] and of chicken hepatocytes, where PDIA3 was found mainly in the internal nuclear matrix fraction [Altieri et al., 1993]. This observation was at first not easily accepted, because it was considered unlikely that a protein provided with an ER retention signal can escape from the endoplasmic reticulum. However, nowadays there is ample experimental evidence, provided by different laboratories with a variety of experimental techniques, that PDIA3 can be found in the nucleus. It has been shown that PDIA3 is present in the nuclei of HeLa cells and that it interacts directly with DNA [Coppari et al., 2002]. PDIA3 interacts preferentially with A/T rich regions, and in general with DNA regions typical of the MARs (nuclear matrix associated regions) [Coppari et al., 2002; Ferraro et al., 1999]. The DNA fragments immunoprecipitated with an anti-PDIA3 antibody from HeLa and Raji cells were enriched in sequences contained either in introns or

in 5'-flanking regions of known genes [Chichiarelli et al., 2007; Chichiarelli et al., 2010]. This can be compatible with a gene expression regulatory function. Furthermore, the consensus sequences for STAT3 were found to be associated both with this transcription factor and with PDIA3 [Chichiarelli et al., 2010]. Because of the relatively low affinity for DNA and its lack of stringent sequence specificity, PDIA3 cannot itself be considered as a transcription factor, but it might be considered an accessory protein for transcription regulation, possibly maintaining the transcription factors in their proper redox state.

Moreover, PDIA3 shows *in vitro* DNA-binding properties that are strongly dependent on the redox state of the protein. The DNA binds to the  $\alpha'$  domain [Grillo et al., 2002] and the binding requires the oxidized form of PDIA3 [Ferraro et al., 1999; Grillo et al., 2007]. Evidences, from M14 melanoma cells and HepG2 hepatoma cells, demonstrated the association of STAT3 and PDIA3 also in the nucleus at the level of DNA interaction [Eufemi et al., 2004; Chichiarelli et al., 2010]. The PDIA3 silencing in M14 cells causes a decrease in the expression of the STAT3-dependent gene *CRP* [Chichiarelli et al., 2010], suggesting the possibility of a positive involvement of PDIA3 in the signalling and/or DNA binding of STAT3.

In NB4 leukemia cells, PDIA3 and NF $\kappa$ B translocate to the nucleus after treatment with calcitriol and phorbol ester [Wu et al., 2010], hypothesizing, again, a role of PDIA3 in the control of gene expression through regulation of the conformation of associated transcription factors.

Finally, PDIA3 displays *in vitro* and *in vivo* affinity for Ref-1, a protein involved in DNA repair as well as in the reduction and activation of transcription factors. These two proteins appear to cooperate in the activation

of a variety of transcription factors, which need to be in their reduced form in order to bind DNA [Grillo et al.,2006].

#### ***1.3.4. PDIA3 on cell membrane and secretion***

The first time in which it was observed that PDIA3 can escape from the ER was when Hirano et al. noticed that the protein was being secreted from 3T3 cells [Hirano et al., 1995]. Afterwards several studies showed that PDIA3 could be found on the cell surface or in complexes with cell membrane proteins.

PDIA3 has been found on the surface of the sperm head, where it is required for sperm-egg fusion [Ellerman et al., 2006]. Possibly the PDIA3 role is related to the thiol-disulfide exchange reactions necessary for the gamete fusion process.

One of the function of PDIA3 on the cell surface is the binding of the hydroxylated, hormonal form of vitamin D3, i.e. 1 $\alpha$ ,25-dihydroxycholecalciferol (1 $\alpha$ ,25-(OH)2D3, calcitriol) [Nemere et al., 2004], followed by activation of non-genomic responses and the internalization and nuclear import of PDIA3 itself.

It has been demonstrated that PDIA3 exists in caveolae, where it interacts with phospholipase A2 (PLA2) activating protein (PLAA) and caveolin-1 to initiate a rapid signalling in musculoskeletal cells via PLA2, phospholipase C (PLC), protein kinase C (PKC) and the ERK1/2 family of mitogen activated protein kinases (MAPK) [Boyan et al., 2012].

Moreover it was recently reported that PDIA3 is associated and co-localizes with  $\beta$ -DG (one of the two subunit of the extracellular receptor dystroglycan, DG) at the plasma membrane of 293-Ebna cells. It has been argued that

PDIA3 may assist DG during its post-translational maturation or that it could modulate DG redox state [Sciandra et al., 2012].

PDIA3 is also present on the platelet surface and it has been showed that its inhibition blocks platelet activation [Holbrook et al., 2012; Wu et al., 2012].

PDIA3 is secreted by platelets and endothelial cells upon vascular injury and accumulates in the thrombus, where it regulates the activation and recruitment of other platelets [Holbrook et al., 2012].

Dihazi et al. [Dihazi et al.,2011] showed that PDIA3 was found to be secreted by renal cells in high amounts upon profibrotic cytokine treatment, and to interact with extracellular matrix (ECM) proteins, such as fibronectin and collagen. These data suggest that secreted PDIA3 could participate in ECM synthesis and stabilization, thus potentially leading to a progressive renal fibrosis.

#### **1.4. PDIA3 and diseases**

PDIA3 has been associated with several human diseases such as cancer, prion disorders, Alzheimer's disease, Parkinson's disease and hepatitis [Hetz et al., 2005; Martin et al., 1993; Muhlenkamp and Gill, 1998; Seliger et al., 2001; Erickson et al., 2005; Tourkova et al., 2005]. PDIA3 expression is increased in transformed cells, and it is thought that its role in oncogenic transformation is directly due to its ability to control intracellular and extracellular redox activities [Hirano et al., 1995]. An increase in PDIA3 expression has also been observed in the early stages of prion disease, suggesting that it may play a neuroprotective role in the cellular response to prion infection [Hetz et al., 2005]. Parkinson's disease is characterized by the progressive loss of dopaminergic neurons of the substantia nigra. It has been

shown that the treatment of cell lines with 6-hydroxidopamine (6-OHDA, a Parkinson mimetic neurotoxin that selectively kills dopaminergic neurons) induces PDIA3 oxidation and PDIA3-DNA conjugates formation. It was suggested that PDIA3 plays an early adaptive response in toxin-mediated stress [Kim-Han et al., 2007].

### ***1.4.1. PDIA3 and Alzheimer's disease***

Alzheimer's disease (AD) is a common neurodegenerative disorder in humans, characterized by deposition in the brain of  $\beta$  amyloid ( $A\beta$ ) plaques and neurofibrillary tangles (NFTs).  $A\beta$  plaques are constituted by  $A\beta$ 1-40 and  $A\beta$ 1-42 peptides, which are the results of the APP (amyloid precursor protein) proteolytic cleavage and are thought to be the main cause of the Alzheimer development [Blennow et al., 2006; Ling et al., 2003]. It has been found that  $A\beta$  is present in Alzheimer's patients plaques only as a naked peptide, while it is complexed to PDIA3 and calreticulin in the cerebrospinal fluid (CSF) of healthy individuals; it was postulated that normally PDIA3 and calreticulin bind to N-glycosylated  $A\beta$  in order to keep it in solution preventing its aggregation and deposition. [Erickson et al., 2005].

It is now widely known that plaque formation is due to the failure of the ER post translational processing of APP [Holtzman et al., 2013]; this condition is also a typical manifestation of aging. In this regard it was found a decrease in PDIA3 levels with age [Erickson et al., 2006] and in N-glycosylated proteins in the tissue of the elderly [Kousvelari et al., 1988]. These findings may give an explanation of what happens in Alzheimer's disease: the decrease in PDIA3 levels could impair its ability to keep  $A\beta$  in solution, even more if  $A\beta$  is not glycosylated due to the reduced cell ability to produce N-glycosylated

proteins. Tohda et al. reported the beneficial effect of diosgenin on the memory deficit in an AD mice model and on retrieval of axonal and presynaptic degeneration in the cerebral cortex and hippocampus, detecting PDIA3 as a target of diosgenin. Interestingly they showed that diosgenin-induced axonal growth was significantly inhibited in primary cortical neurons after PDIA3 knockdown [Tohda et al., 2012].

### **1.5. ER stress and UPR**

The endoplasmic reticulum (ER) is a multifunctional cellular organelle responsible for several functions necessary for cell survival, such as folding, post-translational modification, transportation, and quality control of newly synthesized proteins. Endogenous or exogenous insults can alter ER functions through disruption of calcium and redox homeostasis, glucose starvation and protein misfolding. The result of these alterations is the induction of ER stress [Paschen and Frandsen, 2001; Schroder and Kaufman, 2005; Rao et al., 2004; Breckenridge et al., 2003]. ER stress results in activation of the unfolded protein response (UPR) with the aim to alleviate the stress and to restore the proteostasis. In order to do that, the UPR causes changes in the expression of a huge amount of genes; for instance it causes general translational attenuation, reducing the load of proteins within the ER, and up-regulation of protein chaperones, promoting protein folding, in order to maintain the quality control of proteins while the misfolded proteins get degraded through ER-associated degradation (ERAD) and autophagy. However, in circumstances of chronic or prolonged ER stress, the UPR activates apoptotic signalling, therefore triggering cell death. The UPR is mediated by three ER stress sensors: PKR-like endoplasmic reticulum kinase

(PERK), inositol-requiring kinase 1 (IRE1), and activating transcription factor 6 (ATF6). These sensors induce UPR after the recognition of ER stress/misfolding of proteins. Under normal conditions, these ER stress sensors are bound to the ER chaperone BiP (or GRP-78, glucose-related protein 78), which keeps them in an inactivated state. In presence of ER stress, which leads to accumulation of misfolded proteins in the ER lumen, BiP dissociates from the ER stress sensors to preferentially bind the hydrophobic regions of the misfolded proteins, thus resulting in sensors' activation (Fig. 6) [Rutkowski et al., 2006].

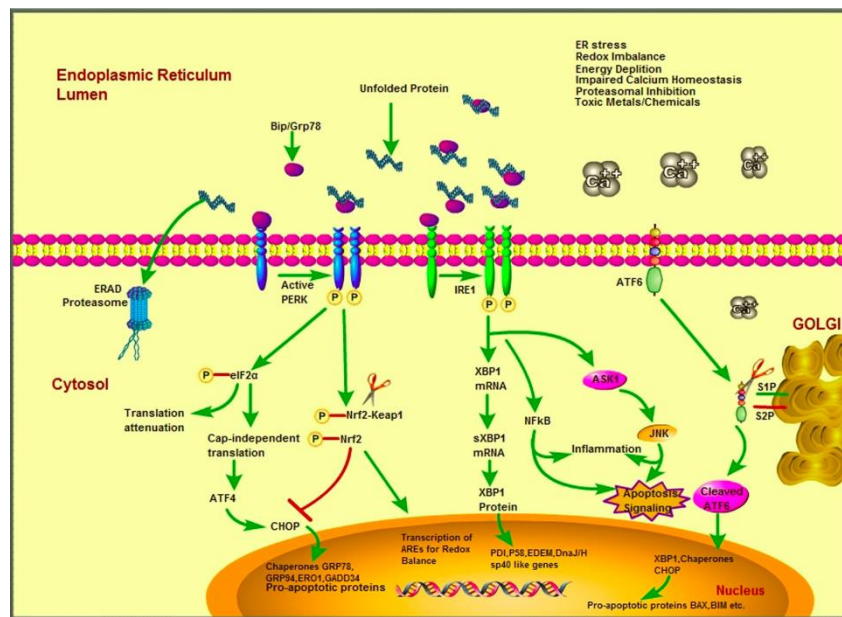


**Figure 6.** A schematic demonstrating the action of the three ER stress sensors on the Unfolded Protein Response. [Mahdi et al., 2016]

Once activated, PERK phosphorylates, and thus inhibits, the ubiquitous eukaryotic translation initiation factor 2 $\alpha$  (eIF2 $\alpha$ ). In this way there is a decrease in the number of newly synthesized proteins into the ER lumen,

therefore reducing the load of ER protein-folding [Boyce et al., 2005]. Phosphorylation of eIF2 $\alpha$  also brings to the translation of the mRNA encoding ATF4. This transcription factor translocates to the nucleus where it induces the expression of ER chaperones to increase refolding of misfolded proteins [Halperin et al., 2014]. ATF4 also induces the expression of various genes involved in autophagy, antioxidant response, amino acid biosynthesis and transport [Cao and Kaufman, 2012; Hetz and Mollereau, 2014]. Under ER stress, ATF6 is activated and then translocates from the ER membrane to the Golgi apparatus where it is cleaved by site-1 and site-2 proteases. The resulting cleaved ATF6 translocates from the cytosol to the nucleus where it induces transcription of ER chaperones, ERAD components and XBP-1 [Schröder and Kaufman, 2005].

### 1.5.1. IRE1

The UPR mediator IRE1 is a transmembrane receptor kinase located on the surface of the endoplasmic reticulum (ER). This protein consists of different domains: the luminal domain, the transmembrane domain (TM), the linker domain, the kinase domain and the endoribonuclease domain (KEN) (Fig. 7) .

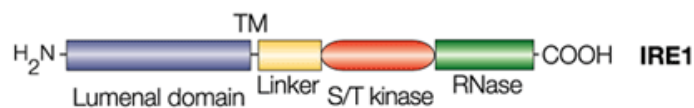


**Figure 7.** Schematic representation of human IRE1. Luminal domain, transmembrane domain (“TM”), linker domain, serine/threonine kinase domain (S/T kinase), and endoribonuclease domain (RNase). [Kaufman et al., 2002]

When ER stress occurs, BIP dissociates from the luminal domain of IRE1; interactions of the stress-sensing luminal domains of two IRE1 monomers [Bertolotti et al., 2000; Credle et al., 2005; Kimata et al., 2007] promotes trans-autophosphorylation of the kinase and RNase domains on the cytoplasmic side of the ER membrane [Ali et al., 2011; Shamu and Walter, 1996]. Phosphorylation allows the binding of nucleotides in a pocket present in the kinase domain. Nucleotide binding triggers conformational changes in IRE1, which stabilize the dimer. This rearrangement in the RNase domain places the residues necessary for the catalysis in the correct orientation [Korennykh et al., 2011]. It is also known that IRE1 can arrange in higher-order oligomers [Korennykh et al., 2009; Li et al., 2010].

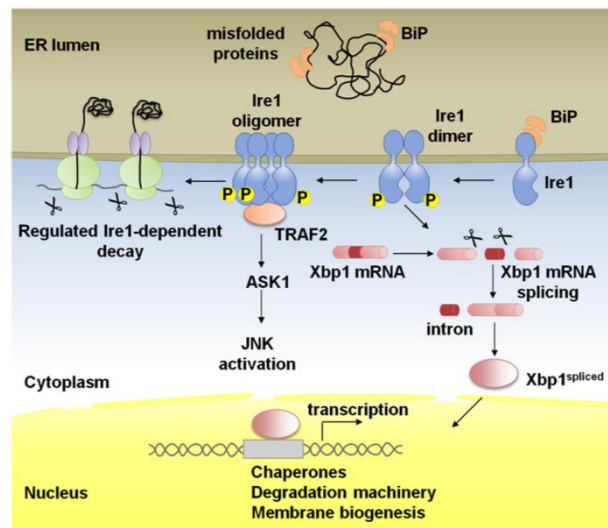


**Figure 8.** Schematic representation of IRE1 signalling pathway. [Coelho and Domingos, 2014]

The active endoribonuclease (RNase) domain of IRE1 cleaves a 26 nucleotide intron of the mRNA coding for the transcription factor XBP1 (X-box binding protein-1) in mammalian cells [Calton et al., 2002; Gonzalez et

al., 1999; Kawahara et al., 1997; Sidrauski and Walter, 1997]. The resulting cleaved exons are then ligated by the RNA ligase RtcB [Lu et al., 2014] in order to obtain the spliced form of the XBP1 mRNA. This potent transcription factor regulates the expression of several genes important for the re-establishment of ER functions; among these there are genes encoding ER-resident molecular chaperones [Lee et al., 2003] and components of the ERAD (ER-associated protein degradation) machinery [Oda et al., 2006; Yoshida et al., 2003]. Activated IRE1 can also cleave a subset of mRNAs encoding proteins targeted to the ER [Han et al., 2009; Hollien et al., 2009; Hollien and Weissman, 2006; Kimmig et al., 2012; Mishiba et al., 2013] In this case the cleavage leads to mRNA degradation; this process has been called regulated IRE1-dependent decay (RIDD) [Hollien et al., 2009]. RIDD regulates many physiological processes, including degradation of mRNAs encoding a subset of ER or secretory proteins prone to misfolding [Hollien and Weissman, 2006; Han et al., 2009; Hollien et al., 2009; Oikawa et al., 2010], regulation of lipid metabolism genes [So et al., 2012] and fatty acid transport proteins [Coelho et al., 2013]. RIDD is also responsible for the degradation of several miRNAs' precursors, such as miR-17, miR-34a, miR-96, and miR-125b with consequent translation of TXNIP (thioredoxin interacting protein) and caspase-2 mRNAs [Lerner et al., 2012; Osowski et al., 2012; Upton et al., 2012]. TXNIP causes activation of caspase-1 and secretion of interleukin 1 $\beta$ , leading to apoptosis [Lerner et al., 2012]. The role of caspase-2 in ER stress-induced apoptosis has been questioned; indeed a report claimed that ER stress did not cause upregulation and activation of caspase-2 [Sandow et al., 2014]. Moreover IRE1, through its kinase domain, activates the c-Jun N-terminal kinases (JNKs) via the formation of a complex

with the E3 ubiquitin ligase TRAF2 (TNF receptor-associated factor 2) and the apoptosis signal regulating kinase 1 (ASK1), leading to apoptosis. [Urano F et al., 2000; Nishitoh H et al., 2002]. IRE1 is not only involved in the attempt to restore ER homeostasis under stress conditions but it also essential for physiological processes requiring high levels of secretion, such as the differentiation of B cells in plasma cells [Zhang et al., 2005] and insulin secretion from pancreatic beta cells. It has been demonstrated in several studies that alteration in IRE1 function occurs in different diseases such as cancer, diabetes, inflammatory and neurodegenerative diseases [Hetz and Glimcher, 2011; Hetz et al., 2011].

It still not entirely known how IRE1 regulates cell fate; in particular, which of IRE1 activities are associated to cell survival and which to cell death. It has been shown that amplitude and duration of its activation plays an important role [Hetz, 2012]. The common thinking is that XBP1 splicing has mostly a prosurvival effect; in fact, it has been observed that high levels of XBP-1(S) increase tumor cell survival [Davies MP et al., 2008], whereas RIDD shows a proapoptotic output that dominates in other diseases, such as diabetes [Hetz and Glimcher, 2011; Hetz et al., 2011]. Nevertheless, the precise mechanisms of these actions need to be further investigated.

## **1.6. Flavonoids**

Flavonoids are a large class of plant secondary metabolites present in fruits, vegetables and plant-based beverages such as tea and red wine [Pérez-Jiménez et al., 2010]. These polyphenolic compounds are classified into flavones, flavonols, isoflavones, flavanones, flavanols and anthocyanidins [Manach et al., 2004; Bravo, 1998] (Fig. 9).

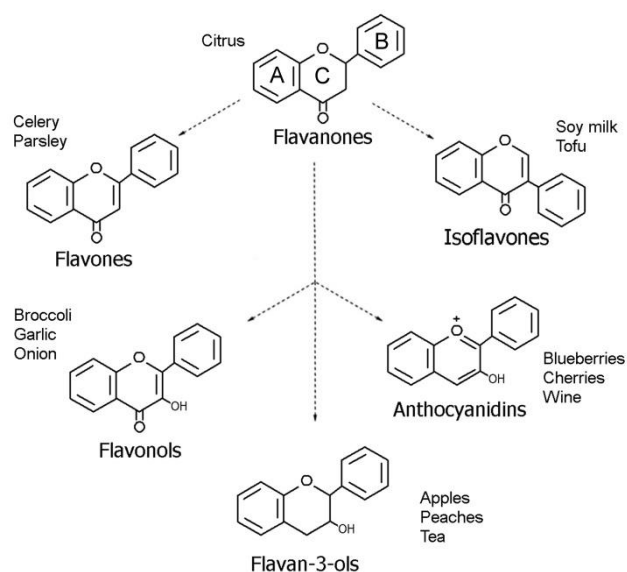


**Figure 9.** Flavonoid structures and occurrence. Arrows indicate biosynthetic path.

Flavonoids show multiple health beneficial effects; many studies have suggested an association between consumption of flavonoids-rich food or beverages and the prevention of many degenerative diseases, including cancer, neurodegeneration and coronary heart disease and stroke [Woo et al., 2013; Neuhouser, 2004; Hui et al., 2013; Aune et al., 2012; Hertog et al., 1993]. The protection offered by flavonoids is believed to be due to their antioxidant activity. The aromatic rings of the flavonoid molecule allow the donation and acceptance of electrons from free radical species [Halliwell, 2006]. It has been suggested that, in lower amounts, flavonoids may exert pharmacological activity within the cells, although for most of them the cellular basis of these activities is not well known. By affecting different pathways, such as cell signalling, cell cycle, free radical scavenging,

angiogenesis, DNA repair mechanisms and apoptosis, flavonoids have the ability to control cell proliferation and survival, and to exhibit antiproliferative and antimutagenic properties and a remarkable anti-inflammatory activity [George et al., 2016; Jayasena et al., 2013; Mandel et al., 2011; Vauzour et al., 2010].

### 2. AIMS OF THE RESEARCH

**AIM 1: to perform a wide screening study to identify specific flavonoid molecules that bind and modulate PDIA3 activity, useful to regulate the cellular processes and signalling pathways involving PDIA3.**

PDIA3 is a multifunctional protein disulfide isomerase with a wide range of functions. It has been shown that this protein is involved in the cellular response to stress as well as in cancer and neurodegeneration. Flavonoids displays a wide range of biological effects, such as antioxidant, anti-inflammatory, antithrombotic, antiviral and antitumor activities. However, for many of them the molecular and cellular bases of these activities are not well known. Flavonoids can act on different targets affecting regulation of a variety of pathways: cell signalling and cell cycle, free radical scavenging, inhibition of angiogenesis, initiation of DNA repair mechanisms, apoptotic induction and inhibition of metastasis. Starting from previous work done in our lab, which showed that green tea catechins are able to modify PDIA3 activity [Trnkova et al., 2013], we expanded this study to various classes of flavonoids and performed a wide screening study for assessing the interaction and impact on PDIA3 protein activity of several types of flavonoids. Our hypothesis is that some of the flavonoids' activities are connected to the modulation of PDIA3 functions. The binding of several flavonoids to PDIA3 and their effects on the protein were tested by protein fluorescence quenching. PDIA3 redox and DNA-binding activities were also analyzed in the presence of flavonoids.

**AIM 2: to study PDIA3 implications in Alzheimer's disease (AD) and  $\beta$ -amyloid deposits.**

Evidences from the literature suggest that PDIA3 might have a role in AD

pathogenesis [Erickson et al., 2005; Tohda et al., 2012], but its exact contribution is not clear. In order to shed light on this interesting question, we mimicked AD pathological conditions by treating a neuronal cell model with  $\beta$ -amyloid peptide and analyzed PDIA3 role in AD. In particular we investigated PDIA3 expression levels through western blot and qRT-PCR analysis, PDIA3 localization by means of immunofluorescence studies and PDIA3 secretion before and after  $\beta$ -amyloid peptide treatment.

**AIM 3: to understand how different IRE1 activities are related to each other, to cell fate under ER stress and to IRE1 protein dimerization and oligomerization.**

The last part of my PhD program was performed at The Children's Hospital of Philadelphia, where I worked under doctor Yair Argon's supervision on the UPR sensor and mediator IRE1, a serine threonine protein kinase that possess endonuclease activity. IRE1 is an ER transmembrane protein essential for developmental processes requiring high levels of secretion, such as the differentiation of plasma cells and pancreatic beta cells. Under normal conditions IRE1 is present as an inactive monomer bound to the chaperone BIP. In response to ER stress, BIP dissociates from IRE1, with consequent IRE1 activation, which consists in dimerization, trans-autophosphorylation, conformational changes and activation of the RNase domain, which affects downstream targets to work as an administrator of cell fate under ER stress.

Following activation, IRE1 has three main activities: XBP1 mRNA splicing; specific mRNAs and miRNAs degradation (RIDD, regulated IRE1 dependent decay) and activation of the JNK pathway through TRAF2 interaction. Together, these activities are responsible for both adaptive responses and apoptosis, but nobody has ever separated each outcome.

## AIMS OF THE RESEARCH

---

It is known that IRE1 can exist in a monomeric state (inactive) or after activation in dimeric and oligomeric (clustering) states. The differences and the functions of these last IRE1 states are still not known and different researchers have only postulated their activities. Our hypothesis is that IRE1 clustering is related to two activities of IRE1: RIDD and activation of the JNK-pathway, which are commonly believed to have a pro-apoptotic outcome following ER stress, but not to XBP1 mRNA splicing, which activates pro-survival responses. To investigate this aspect we used an IRE1 knock-out cell line, reconstituted with a recombinant GFP-tagged human IRE1, either as wild type version or containing several point mutations. Our goal was to find IRE1 mutant proteins that can perform one activity but not the other ones to allow us to connect the different outcomes to each activity. In this part we focused our attention mainly on XBP1 splicing and clustering, leaving the study of RIDD and JNK pathway activation for further studies.

## 3. MATERIALS AND METHODS

### 3.1. Reagents

PBS solution, acrylamide, N-ethylmaleimide, DTT, GSSG, eosin isothiocyanate and different flavonoids (quercetin, 3-O-methyl-quercetin, isoquercetin, quercitrin, rutin, morin, rhamnetin, isorhamnetin, fisetin, apigenin, apigenin-7-glucoside, luteolin-7-glucoside, kaempferol, eupatorin, eupatorin-5-methyl-ether, genistein, narigenin, cyanidin and 6,2',4'-trimethoxyflavone), cycloheximide, brefeldin A, doxycycline hydrochloride and MG-132 were from Sigma-Aldrich; thapsigargin and tunicamycin from Calbiochem; EDTA (0.5 M solution pH 8.0) from IBI Scientific. Amyloid beta peptide 25–35 fragment (A $\beta$ 25–35), synthesized by conventional solid phase chemistry [Atherton and Sheppard, 1989], was aggregated overnight at 37°C in phosphate buffered saline at a concentration of 1mM.

### 3.2. Protein expression and purification

Human recombinant PDIA3 was cloned and expressed in *E. coli* strain BL21 using the expression vector pET21 (Novagen) as previously described [Coppari et al., 2002]. The coding sequence for the second redox-active domain (a' domain, residues 377-505) was amplified by PCR as previously described and cloned in the expression vector pET29 (Novagen) [Grillo et al., 2007]. Recombinant proteins were expressed in *E. coli* strain BL21 and purified by ammonium sulphate fractionation, ion exchange and heparin chromatography [Grillo et al., 2006; Grillo et al., 2007]. Protein purification was evaluated by SDS-PAGE and concentration was determined spectrophotometrically (PDIA3  $\epsilon$ 280 reduced form = 44,810 M<sup>-1</sup>cm<sup>-1</sup>, a'

domain  $\epsilon_{280}$  reduced form = 14,400 M<sup>-1</sup>cm<sup>-1</sup>).

### 3.3. Fluorescence Quenching Measurements

Quantitative analysis of the interaction between individual flavonoids and PDIA3 was performed by fluorimetric titration. Fluorescence spectra were recorded using a SPEX-FluoroMax spectrofluorimeter (Horiba Scientific) from 300 to 500 nm with excitation at 290 nm using a 10 mm path length quartz fluorescence cuvette and under continuous stirring. The excitation and emission slits were both set to 5 nm and scan speed was 120 nm·min<sup>-1</sup>. Briefly, solution of PDIA3 (0.5  $\mu$ M) or a' domain (1  $\mu$ M) in phosphate buffered saline (PBS) containing DTT 0.1 mM and EDTA 0.2 mM were titrated in quartz cuvette by stepwise additions, at 5 min time intervals, of individual flavonoid solution (1 mM in PBS/ethanol 50:50 v/v freshly prepared from a 20 mM stock solution in DMSO). Most of tested flavonoids can absorb light at the excitation and emission wavelengths. To minimize the inner-filter effect we limited the highest concentration reached in the titration test up to 10  $\mu$ M. All experiments were carried out at 25°C. Each spectrum was the mean of three repeated scans. Fluorescence spectra of appropriate blanks (flavonoids without proteins) were recorded under the same experimental conditions and subtracted from the corresponding flavonoid-protein system to correct the fluorescence background. Fluorescence intensities recorded at 338 nm were used for quenching analysis and data obtained for each flavonoid are the average of at least three independent titration experiments.

### **3.4. Determination of Protein Disulfide Reductase Activity**

Disulfide reductase activity of PDIA3 was monitored by sensitive fluorescent assay using eosin glutathione disulfide (DiE-GSSG) as fluorogenic probe [Raturi A and Mutus B, 2007]. DiE-GSSG was synthesized by the reaction of eosin isothiocyanate with oxidized glutathione (GSSG) according to the method of Raturi and Mutus [Raturi A and Mutus B, 2007] with some modifications [Trnkova et al., 2013]. DiE-GSSG concentration was determined spectrophotometrically ( $\epsilon_{525} = 88,000 \text{ M}^{-1}\text{cm}^{-1}$ ). Disulfide reductase activity was assayed in a reaction buffer containing 2 mM EDTA, 150 nM DiE-GSSG and 5  $\mu\text{M}$  DTT in PBS. A 20  $\mu\text{l}$  aliquot of a stock solution of PDIA3 (1 $\mu\text{M}$ ) was added to the reaction mixture and DiE-GSSG reduction was monitored at 545 nm with excitation at 520 nm, at 25°C with continuous stirring. Reductase activity was calculated as the initial velocity in fluorescence increase. To test the effect of flavonoids on PDIA3 activity, the protein stock solution was previously incubated for 15 minutes at room temperature with different concentrations of each flavonoid and then a 20  $\mu\text{l}$  aliquot subjected to assay in a reaction buffer containing the same concentration of the flavonoid.

### **3.5. Determination of DNA Binding Activity by EMSA**

EMSA assay was performed using a 79-bp rich DNA fragment obtained by PCR as previously described [Grillo et al., 2002]. Amplified DNA was end-labeled by using 5-fluorescein-modified primers. 10 ng of DNA fragment was incubated with 1  $\mu\text{g}$  of PDIA3 or a' domain, in presence of increasing concentration of flavonoids (from 0 to 50  $\mu\text{M}$ ). Controls were performed

using DNA alone and in the presence of each flavonoid. All tests were performed in 20  $\mu$ l mixtures containing 20 mM Tris-HCl, pH 7.5, 50 mM NaCl, and 10 % (v/v) glycerol. Samples were incubated for 1 hour at 25° C and then resolved on 5% polyacrylamide gels in 0,25% TBE buffer (22.5 mM Tris-borate, 5 mM EDTA, pH 8.3) at 150 V. Gel images were recorded using a ChemiDoc MP Imaging System (BioRad) equipped with an epi-blue excitation lamp and a 520nm emission filter.

### **3.6. Statistical analysis**

Fluorescence quenching constant ( $K_{SV}$ ) values were given as means  $\pm$  standard deviation and values of disulfide reductase activity were expressed in % of control sample  $\pm$  relative standard deviation. All measurements were performed at least three times. Dunnett's test was used to compare the obtained reductase activity data with the activity of the untreated protein and a p-value of  $< 0.01$  was considered as statistically significant.

### **3.7. Cell cultures**

SH-SY5Y cells were grown in Ham's F12/DMEM; HAP1 cell line was grown in IMDM; 293T cells were grown in DMEM. All the media were supplemented with 10% FBS (fetal bovine serum), 100 units/ml penicillin, 100 g/ml streptomycin, 1mM sodium pyruvate, 2mM glutamine. All cells were grown to 70-80% confluence at 37° C with 5% CO<sub>2</sub>.

### **3.8. Cell lysate preparation**

Adherent cells were washed and scraped with cold PSB. Then, they were

## MATERIALS AND METHODS

---

harvested by centrifugation and suspended in lysis buffer (50mM Tris pH 8.0, 150mM NaCl, 20mM iodoacetamide, 5mM KCl, 5mM MgCl<sub>2</sub>, 1% NP-40) supplemented with protease and phosphatase inhibitor cocktails (PhosSTOP™ from Roche). After centrifugation (15min, 20.000g, 4°C), the total protein extracted were quantify using Pierce™ BCA Protein Assay Kit (Thermo Fisher Scientific), and resuspended in 1X Laemmli Buffer ( 2% SDS, 62,5 mM Tris-HCl pH 6.8, 10% v/v glycerol, 5 mM DTT, 0.02% bromophenol blue) for the electrophoresis.

### **3.9. Proteins precipitation in culture medium**

After growing SH-SY5Y cells on 6-wells plates, the media was taken, subjected to 5,000 rpm for 5 minutes to remove cells and the supernatant was treated with 0.025% sodium deoxycholate, 10% trichloroacetic acid (TCA) over night at 4° C. The day after samples were centrifuged at 10,000 rpm for 15 minutes at 4° C , a wash in 100 µl of acetone was performed, 10,000 rpm for 15 minutes at 4° C centrifugation and air dried. The pellets were resuspended in Laemmli buffer 1X.

### **3.10. Western blot**

Samples in 1X Laemmli buffer were boiled for 5 minutes. Immunoblotting was performed using the PPDS module of the Owl Separation System™ (Thermo) and 10% 37.5:1 Acrylamide/Bis-Acrylamide poly-acrylamide gels. SDS-PAGE was performed using Tris-Glycine-SDS buffer and transferred onto 0.45um nitrocellulose membrane (Biorad) in Tris-Glycine buffer plus 20% methanol, using a Genie™ Blot Module (Thermo). Nitrocellulose

membranes were blocked in 5% non-fat milk in TBS buffer. The blots were then incubated overnight at 4°C, in 1% non-fat milk/TBS-0.1% Tween (TBS-T) plus the primary antibody. Afterward the membranes were washed in TBS-T and incubated with the appropriate infrared (IR) labeled secondary antibody (Licor) in 5% milk/TBS-T. The membranes were washed and scanned using the Odyssey® Infrared Imaging System (Licor). Protein bands were visualized and densitometry determined by Image J software.

Rabbit anti-IRE1 (14C10) was purchased from Cell Signaling Technology. Rabbit anti-phospho Ser 724 IRE1 was purchased from Novus Biologicals. Rabbit anti-PDIA3 was purchased from Millipore. Mouse anti  $\beta$ -actin was purchased from Sigma-Aldrich. Mouse anti-BiP antibody was purchased from BD Transduction Laboratories. IR secondary antibodies (used at 1:10000 dilutions) were from Licor.

### **3.11. Cell viability assay**

Cellular proliferation was examined employing an XTT-based colorimetric assay according to the manufacturer's protocol. Briefly, each of the cells was cultured in 96-well plates. After incubation periods of 24 hours, a XTT Cell Viability Assay Kit (Biotium) was added to each well and incubation was continued for 4 hours at 37°C. Optical density was measured at a wavelength of 450 nm using a 96-multiwell microplate reader (BioTek).

### **3.12. Immunofluorescence**

Cells were grown on glass coverslips (in 6-wells plates, 200,000 cells/well in 2ml of medium) and the day after they were treated with A $\beta$  peptide for 24 hours. Afterwards cells were fixed with 4% formaldehyde for 20 minutes,

## MATERIALS AND METHODS

washed 3 times in PBS, permeabilized with 0.2% Triton X-100 for 15 minutes, washed 3 times with PBS and blocked with 1% w/v BSA (bovine serum albumin) over night at 4° C. Immunostaining was performed incubating cells with anti-PDIA3 antibody (1:100) for 1 hour, washing 3 times in PBS, incubating with TRITC-conjugated secondary antibody (1:200) (Amersham), then washing again 3 times in PBS. Nuclei were stained with DAPI 50 ng/ml for 10 minutes. After washing with PBS, glass microscope slides, mounted with ProLong® Gold Antifade Reagent (Invitrogen), were examined by fluorescence microscopy.

### **3.13. Mutagenesis, lentiviral production and infection**

IRE1-sfGFP was previously cloned in pLVX-Tight-Puro vector by PCR in Yair Argon's lab. Site-directed mutagenesis was performed using the QuikChange II Site-Directed Mutagenesis Kit (Agilent) to generate the following IRE1-GFP mutants: D123P - K907A - L827P. To generate viral particles carrying the expression plasmids, 293T cells were co-transfected with a mix of packaging plasmids (Invitrogen) and DNA of interest using Lipofectamine 2000 (Life Technologies). The next day, the medium was replaced with fresh medium. After 24 hours the supernatant was collected and subjected to a low-speed centrifugation step to remove any remaining cellular debris. Following filtration with a 0.45 µm filter, the lentiviral particles were concentrated with Amicon Ultra-15 10K filters (Millipore). Lentiviral titration was conducted as described in ViraPower™ Lentiviral Expression Systems User Manual (Invitrogen). IRE1-complemented IRE1-/- HAP1s were generated by two consecutive transductions with lentiviral particles carrying pLVX-Tet-On™ or pLVX-Tight-Puro™ plasmids

(Clontech) at a multiplicity of infection (MOI) = 1. When required, the following antibiotics were used to select stable cell clones: 2 µg/mL puromycin (Invivogen), 1 mg/mL G418 (Gemini). Pools of transfectants were then induced with 1µg/mL doxycycline to express IRE1-GFP or its mutants.

### **3.14. Knockdown of PDIA3**

The viral-based RNAi was conducted with PDIA3 shRNA and shRNA control vector clones were from the Mission shRNA library (Sigma). 293T were cultured in 6-well plates and transduced with lentiviral particles encoding the shRNA sequences, packaged using the VeraPower kit (Invitrogen). After 24 h the cells were selected with puromycin as above.

### **3.15. Total RNA extraction, and Reverse Transcription-PCR**

Cells were harvested and total RNA was isolated with TRIzol® Reagent (Invitrogen) following the manufacturer's instructions. RNA was precipitated by adding isopropanol and subsequently centrifuged at 12,500 g for 10 minutes at 4° C. The precipitated RNA was washed with 75% ethanol and air dried. Total RNA was then resuspended in RNase-free water and quantified using Thermo Scientific NanoDrop 2000. Purified RNA was subjected to reverse transcription using Superscript® First Strand Synthesis System for RT-PCR (Invitrogen), according to manufacturer's instructions.

### **3.16. Real-time PCR**

qRT-PCR was performed starting from cDNA using SYBR® Select Master

## MATERIALS AND METHODS

Mix (Applied Biosystems), according to manufacturer's instructions and through StepOnePlus™ Real-Time PCR System (Applied Biosystems). Genes' expression was evaluated using the following primers:

PDIA3: forward: GCCACAGTCTTGTCCTCAAACCTG;  
reverse: TTCCTAAAAGCAGCCAGCAACTTG.

CHOP: forward: GGAGCTGGAAGCCTGGTATG;  
reverse: AAGCAGGGTCAAGAGTGGTG

XBP1 spliced: forward: CTGAGTCCGCAGCAGGTG;  
reverse: GACCTCTGGGAGTTCCTCCA

$\beta$ -actin: forward: GCGAGAAGATGACCCAGATC;  
reverse: GGA TAGCACAGCCTGGATAG.

### 3.17. XBP1 splicing assay

Cells were lysed and total RNA was collected. PolyA mRNA was reverse transcribed using the SuperScript-RT system (Invitrogen). cDNA was used as template for PCR amplification across the fragment of the Xbp-1 cDNA bearing the intron target of IRE1 $\alpha$  ribonuclease activity. The primers used for the PCR are the following:

Fwd: AAACAGAGTAGCAGCTCAGACTGC  
Rev: TCCTTCTGGGTAGACCTCTGGGAG

PCR products, resolved on a 3% agarose/1 $\times$ TAE gel, consist of three amplicons corresponding to unspliced (474 nucleotides) and spliced XBP1 (474 nucleotides), and a hybrid product consisting of unspliced XBP-1 annealed to spliced XBP-1. This hybrid species was also produced through

the PCR and was visible as a slower migrating band above the unspliced amplicon. Ethidium bromide (Sigma) stained amplicons were quantified by densitometry using ImageJ software (NIH).

### **3.18. Live Cell Imaging**

IRE1-complemented IRE1 KO HAP1 cells were seed two days before imaging onto glass-bottom microwell dishes (MatTek) at  $1 \times 10^5$  cells/dish. Doxycycline containing medium was added for 24 h, withdrawn before imaging and replaced with IMDM media without phenol red. Images were acquired with a 63X NA oil objective on a fluorescence inverted microscope equipped with a 37°C environmental chamber.

## 4. RESULTS AND DISCUSSIONS

### 4.1 Comparative analysis of the interaction between different flavonoids and PDIA3

#### *4.1.1 Flavones eupatorin and eupatorin-5-methyl ether bind PDIA3 with high affinity*

We started a screening analysis to find molecules that can specifically bind PDIA3 and inhibit its redox activity. A number of flavonoids, comprising flavones, flavonols and several derivatives, which differ in terms of skeleton structure as well as hydroxyl-, methoxyl- and other substituted groups, were analyzed (Fig. 10).

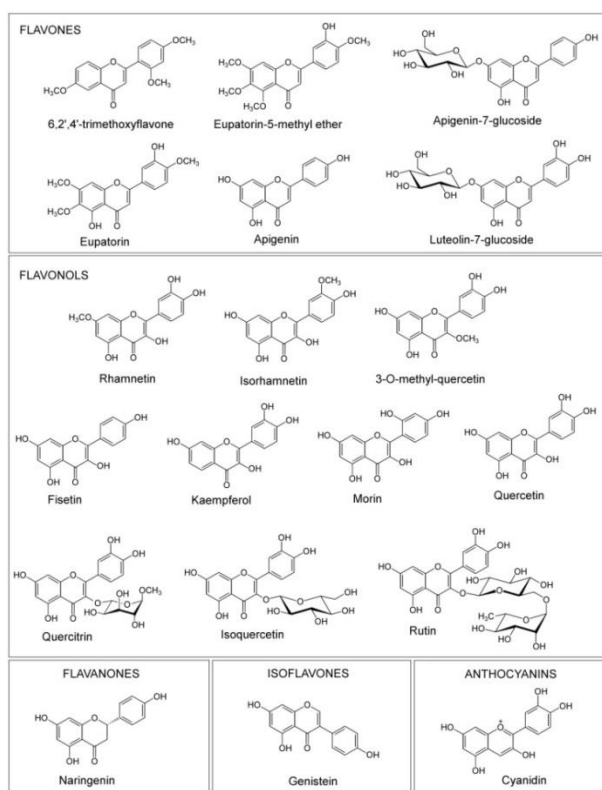


**Figure 10.** Molecular structures of tested flavonoids.

## RESULTS AND DISCUSSIONS

The interaction between PDIA3 and these flavonoids was investigated by quenching analysis of PDIA3 intrinsic fluorescence. PDIA3 fluorescence is mainly due to the presence of three tryptophan residues: one (W279) is buried in a hydrophobic pocket in the b' domain whereas the other two (W56 and W405) are present on the protein surface close to the thioredoxin-like active sites within *a* and *a'* domains, respectively.

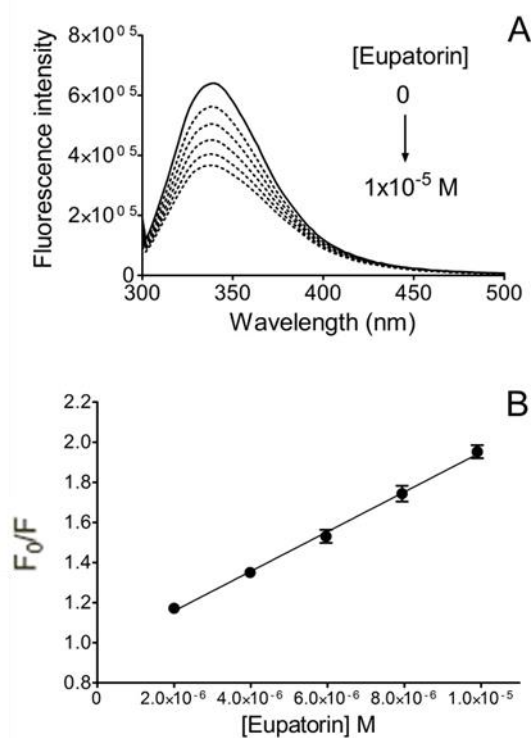


**Figure 11.** (A) Fluorescence quenching spectra of reduced PDIA3 alone (solid line) and after stepwise addition of Eupatorin (dotted line) (pH 7.4, 25°C, and  $\lambda_{\text{ex}} = 290$  nm.). [PDIA3] =  $0.5 \times 10^{-6}$  M, [eupatorin] =  $2 \times 10^{-5}$  M final concentration. (B) Stern-Volmer plot of quenching data as mean of at least three independent experiments (standard deviations were better than 10% and correlation coefficient were better than 0.99).

Quenching analysis was performed on PDIA3 (0.5  $\mu$ M) in the reduced form, by adding stepwise increasing concentration of each molecule and recording the protein fluorescence spectra. For some flavonoids the analysis was

## RESULTS AND DISCUSSIONS

extended to isolate a' domain (1  $\mu$ M), always in the reduced form. Quenching effect on protein as well as Stern-Volmer quenching constants ( $K_{SV}$ ) were calculated from the fluorescence intensities at 338 nm of protein alone ( $F_0$ ) and in the presence of increasing concentration of each ligand molecule ( $F$ ) using the Stern-Volmer equation [Lakowicz, 2006]:

$$F_0/F = 1 + K_{SV}[L]$$

where  $L$  is the ligand concentration. For each ligand molecule the Stern-Volmer quenching constant was obtained by linear regression of plots of  $F_0/F$  versus  $[L]$ . Representative fluorescence spectrum of PDIA3 in the presence of increasing concentration of eupatorin is showed in figure 11a. Fluorescence quenching data were analyzed using the Stern-Volmer equation. The Stern-Volmer plot for PDIA3, in presence of eupatorin, is displayed in figure 11b while the estimated  $K_{SV}$  values of all tested flavonoids are summarized in Table 1 and graphed in figure 12.

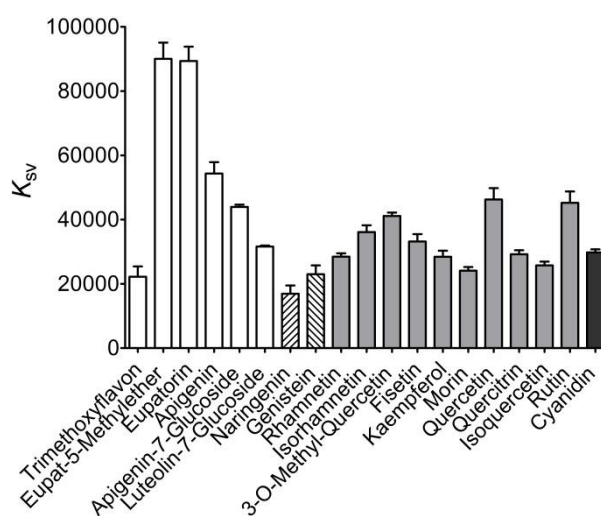


**Figure 12.** Estimated  $K_{SV}$  values of all tested flavonoids obtained by fluorescence quenching analysis of reduced PDIA3 [ $0.5 \times 10^{-6}$  M] in presence of increasing concentration of flavonoids (up to  $2 \times 10^{-5}$  M). Data are reported as mean and standard deviation of at least three independent experiments.

## RESULTS AND DISCUSSIONS

As shown in figure 12, a different degree of quenching was observed in presence of all tested molecules. The decrease of fluorescence may indicate that the microenvironments of tryptophan residues in PDIA3 were altered due to the interaction with tested compounds. The apparent binding constants ( $K_b$ ) and the number of binding sites ( $n$ ) were calculated using the equation described by Bi et al. [Bi et al., 2005], as previously reported [Trnkova et al., 2013]:

$$\log((F_0 - F)/F) = n \log K_b - n \log(1/([L] - n(F_0 - F)[P]/F_0))$$

where  $F_0$  and  $F$  are the fluorescence intensities at 338 nm before and after the addition of the quencher,  $[L]$  and  $[P]$  are the ligand and the total protein concentrations, respectively. The number of binding sites ( $n$ ) and the binding constant ( $K_b$ ) were obtained by plotting  $\log((F_0 - F)/F)$  versus  $\log(1/([L] - n(F_0 - F)[P]/F_0))$  using the reiterative calculation process described by Sun et al. [Sun et al., 2010], assuming a similar affinity for each binding site. The dissociation constant was calculated from the binding constant ( $K_d = 1/K_b$ ).

The estimated  $K_{SV}$ ,  $K_b$  and  $K_d$  values that characterize the interaction of PDIA3 with tested flavonoids are summarized in Table 1.

From our data it is evident that the protein binds most of the tested substances, with an estimated dissociation constant within the  $10^{-5}$  M range. However two molecules are characterized by the highest binding constants: eupatorin and eupatorin-5-methyl ether, with a  $K_d$  around  $1.0 \times 10^{-5}$  M, followed by apigenin with a  $K_d$  of  $1.7 \times 10^{-5}$  M. These molecules, showing the highest affinity toward PDIA3, display an intermediate hydrophilicity degree, if compared with the other flavonoids tested in this study. These observations suggest that a specific degree of hydrophilicity is required to stabilize the interaction of the flavone backbone with the protein.

## RESULTS AND DISCUSSIONS

**Table 1.** Data were calculated from fluorescence quenching analysis using  $0.5 \cdot 10^{-6}$  M PDIA3 in reduced conditions (pH 7.4, 25°C) and increasing concentration (0 to  $10 \cdot 10^{-6}$  M) of different flavonoids.  $K_{SV}$  are reported as mean and standard deviation of at least three independent experiments. The number of binding sites ( $n$ ), the binding constant ( $K_b$ ) and the dissociation constant ( $K_d$ ) were estimated using the equation described by Bi et al. [Bi et al., 2005] and the reiterative calculation process described by Sun et al. [Sun et al., 2010].

Flavonoid	$K_{SV}$ ( $M^{-1}$ )	$n$	$K_b$ ( $M^{-1}$ )	$K_d$ (M)
<u>Flavone</u>				
Trimethoxyflavon	22209 ± 484	0,897	18123	$5,52 \cdot 10^{-5}$
Eupatorin-5-methylether	90016 ± 1875	1,079	90440	$1,11 \cdot 10^{-5}$
Eupatorin	89362 ± 688	1,163	96729	$1,03 \cdot 10^{-5}$
Apigenin	54332 ± 1185	1,083	58739	$1,70 \cdot 10^{-5}$
Apigenin-7-glucoside	43961 ± 673	1,060	47287	$2,11 \cdot 10^{-5}$
Luteolin-7-glucoside	31601 ± 484	1,061	34557	$2,89 \cdot 10^{-5}$
<u>Flavanone</u>				
Naringenin	16900 ± 352	1,053	17295	$5,78 \cdot 10^{-5}$
<u>Isoflavone</u>				
Genistein	22953 ± 435	1,085	24409	$4,10 \cdot 10^{-5}$
<u>Flavonol</u>				
Rhamnetin	28462 ± 295	1,034	30110	$3,32 \cdot 10^{-5}$
Isorhamnetin	36109 ± 1271	0,955	32516	$3,08 \cdot 10^{-5}$
3-O-methyl-quercetin	41110 ± 794	1,090	45719	$2,19 \cdot 10^{-5}$
Fisetin	33164 ± 542	1,076	36862	$2,71 \cdot 10^{-5}$
Kaempferol	28423 ± 982	0,968	26000	$3,85 \cdot 10^{-5}$
Morin	24063 ± 265	1,035	25613	$3,90 \cdot 10^{-5}$
Quercetin	46226 ± 1406	0,877	38987	$2,56 \cdot 10^{-5}$
Quercitrin	29211 ± 483	1,068	32288	$3,10 \cdot 10^{-5}$
Isoquercetin	25738 ± 367	1,077	29073	$3,44 \cdot 10^{-5}$
Rutin	45197 ± 465	0,960	45527	$2,20 \cdot 10^{-5}$
<u>Anthocyanin</u>				
Cyanidin	29761 ± 635	0,992	29257	$3,42 \cdot 10^{-5}$

We also observed that apigenin, genistein and naringenin that share similar functional groups, show different affinity for PDIA3. This difference could be explained by the specific position and orientation of the B ring. In naringenin the B ring on the C2 position is differently oriented respect to A and C rings while it is also differently positioned (C3) in genistein if compared with apigenin (3D models of default conformers are shown in Fig. 13).

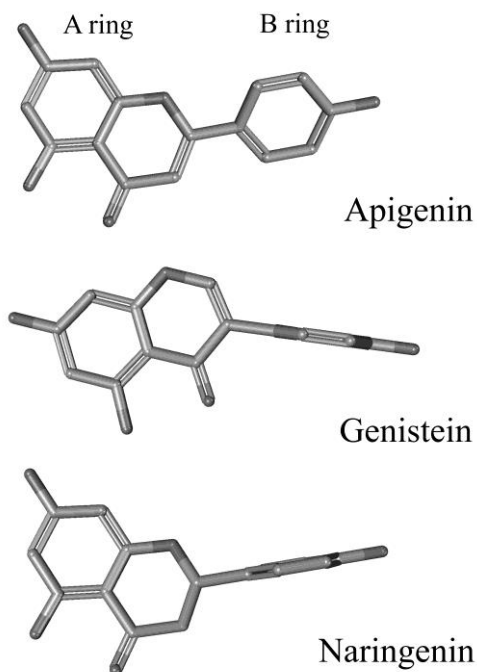


**Figure 13.** 3D models of default conformers for apigenin (CID 5280443), genistein (CID 5280961) and naringenin (CID 932) generated by PubChem (<https://pubchem.ncbi.nlm.nih.gov>).

Hence, it can be hypothesized that the more parallel orientation between the aromatic rings A and B, mainly evident in flavones, is an important feature for the binding to PDIA3.

For some flavonoids, the binding analysis was also extended to the isolated *a'* domain. Similar values for the binding constants were estimated, with some flavonoids showing a slightly better affinity for the whole protein respect to the isolated domain. Even in this case, the molecules that show the greatest affinity are the flavones eupatorin, eupatorin-5-methyl ether and apigenin.

## RESULTS AND DISCUSSIONS

**Table 2.** Dissociation constant ( $K_d$ ) were calculate from fluorescence quenching analysis using  $1 \cdot 10^{-6}$  M a' domain and increasing concentration of different flavonoids.

Flavonoid	$K_d$ (M)
<u>Flavone</u>	
Eupatorin-5-methylether	$1,56 \cdot 10^{-5}$
Eupatorin	$1,62 \cdot 10^{-5}$
Apigenin	$1,71 \cdot 10^{-5}$
<u>Flavonol</u>	
Rhamnetin	$3,04 \cdot 10^{-5}$
Isorhamnetin	$2,95 \cdot 10^{-5}$
3-O-methyl-quercetin	$1,94 \cdot 10^{-5}$
Fisetin	$2,66 \cdot 10^{-5}$
Morin	$3,58 \cdot 10^{-5}$
Quercetin	$3,11 \cdot 10^{-5}$
Quercitrin	$3,01 \cdot 10^{-5}$
Isoquercetin	$4,38 \cdot 10^{-5}$
Rutin	$2,69 \cdot 10^{-5}$

### *4.1.2 Effect of flavonoids on the PDIA3 redox activity*

To verify if the interaction between flavonoids and PDIA3 may have an effect on protein functions, the disulfide reductase activity was tested. For most of the analyzed molecules the effect on the redox activity of the protein was negligible. However, some flavonoids, in particular the flavones eupatorin and eupatorin-5-methyl ether, showed an evident inhibitory effect, up to 40%. Others, such as morin, quercetin and cyanidin, had a less marked inhibition, approximately 20% (Fig. 14).

Apigenin, which showed a binding affinity close to eupatorin, had no evident effect on the protein activity. It is possible that the less polar degree, that characterizes eupatorin and eupatorin-5-methyl ether, may play a significant role.

## RESULTS AND DISCUSSIONS

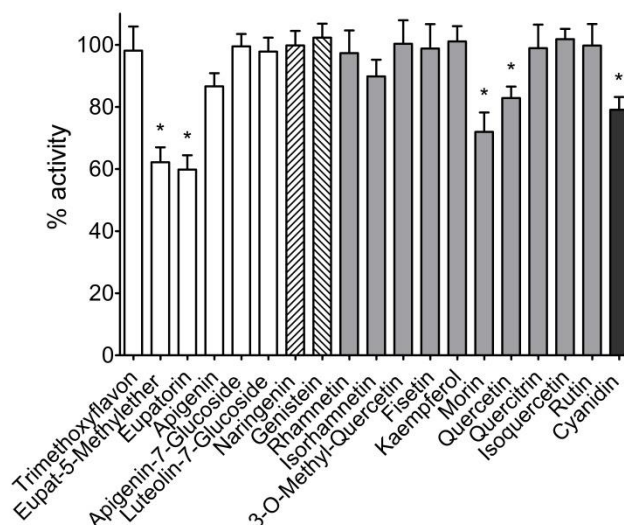


**Figure 14.** Comparison of flavonoid effect (at 20  $\mu$ M concentration) on PDIA3 reductase activity. Plots are displayed as mean and standard deviations of at least six independent measurements. Data were analyzed by Dunnett's test comparing PDIA3 activity in presence of each flavonoid with the activity of untreated protein. Significant differences ( $p < 0.01$ ) are marked with asterisks.

On the basis of these results, we hypothesize that, at least for those molecules showing a marked inhibitory effect on redox activity, the contact region of interaction between the flavonoid structure and PDIA3 should involve the active site. However, since we used a simple substrate like DiE-GSSG to measure the redox activity, we cannot exclude that the inhibitory effect of all flavonoids could be different towards more physiological substrates.

### ***4.1.3 Effect of flavonoids on the DNA binding property of PDIA3***

We also evaluated by EMSA analysis the effect of flavonoids on the DNA binding property of the protein (data not shown). None of tested flavonoids showed an appreciable effect on the DNA binding activity of the protein, differently from what previously reported for galloylated catechins [Trnkova

## RESULTS AND DISCUSSIONS

et al., 2013]. The presence in these molecules of a galloyl moiety linked to the C3 position is probably responsible for a different type of interaction that may extend to a protein region important to the contact with DNA (Fig. 15).

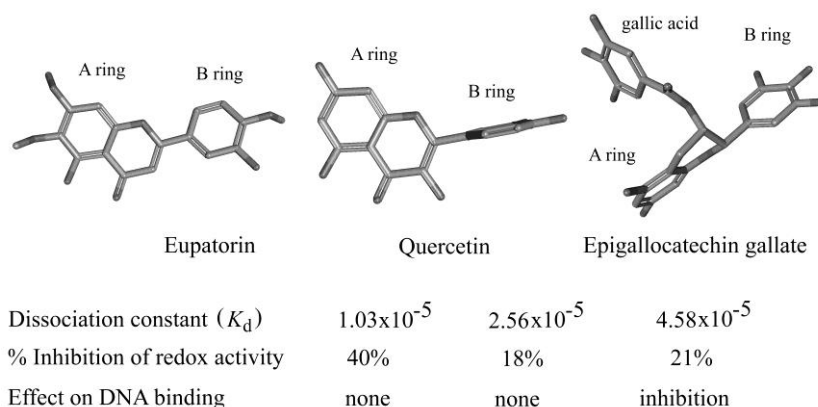


**Figure 15.** 3D models of default conformers for eupatorin (CID 97214), quercetin (CID 5280343) and epigallocatechin gallate (CID 65064) generated by PubChem. The estimated  $K_d$  values that characterize the interaction of PDIA3 with the three flavonoids, the percentage of inhibition of protein redox activity and the effect on DNA binding are also reported (epigallocatechin gallate data were from Trnkova et al., 2013).

In that case, we hypothesized that the galloyl moiety on the C3 position could prevent the DNA binding activity interacting with a  $\beta$ -strand region close to the redox active site. Upon protein oxidation, such region can undergo to a conformational change that is essential for the interaction with the DNA [Grillo et al., 2007]. In this report none of the molecules analyzed have such effect. So we suggest that flavonoids interact with the same protein region containing the tryptophan residues close to the active sites, as suggested from the quenching measurements. However, this interaction may differently extend depending on the flavonoid structure and on specific contacts between flavonoids functional groups and aminoacidic residues on the protein surface.

## 4.2 Involvement of PDIA3 in $\beta$ -amyloid deposits

### *4.2.1 $\beta$ -amyloid peptide treatment causes a decrease in PDIA3 protein but not in mRNA levels in SH-SY5Y cells*

To study the involvement of PDIA3 in  $\beta$ -amyloid deposits and in Alzheimer's disease [Erickson et al., 2005; Tohda et al., 2012], we used SH-SY5Y as a model of neuronal cell line and we treated them with the 25-35 fragment of the amyloid  $\beta$  peptide. This peptide is highly toxic, displays extremely rapid aggregation, enhanced neurotoxicity and increases oxidative stress. First of all, we assessed the viability of SH-SY5Y under increasing concentrations of A $\beta$ 25-35.

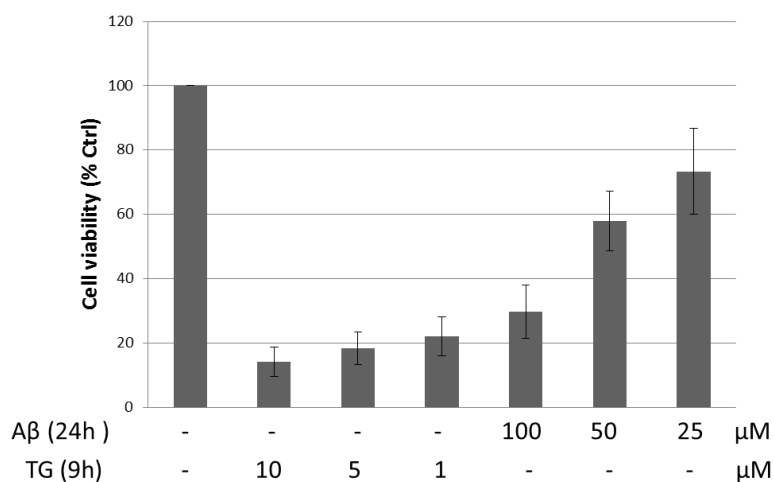


**Figure 16.** Cell viability of SH-SY5Y after exposure to A $\beta$ 25–35 and thapsigargin (Tg) for 24h. The graph is the result of the average of three independent experiments.

As shown in figure 16, A $\beta$ 25-35 treatment decreased cell viability of SH-SY5Y cells in a concentration dependent manner. The ER stress activator

## RESULTS AND DISCUSSIONS

thapsigargin was used as positive control. Given this result for the next experiments we decided to use the amyloid  $\beta$  peptide at a concentration of 50 $\mu$ M.

SH-SY5Y cells were treated with 50 $\mu$ M A $\beta$ 25-35 for 24 hours and after cell lysis the expression levels of PDIA3 were analysed through western blot.

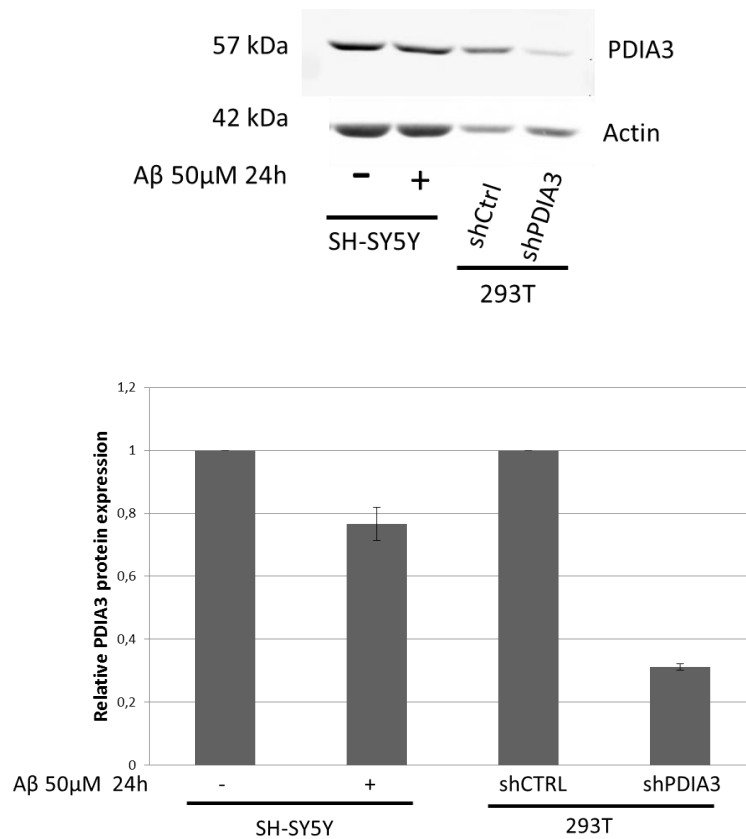


**Figure 17.** Proteins were extracted from SH-SY5Y cells before and, after treatment with 50  $\mu$ M A $\beta$ 25-35 (A $\beta$ ) for 24hours, subjected to western blot analysis and revealed with different antibodies: anti-PDIA3 (on the top) and anti- $\beta$ actin (on the bottom). 293T cells PDIA3 silenced (shPDIA3) and 293T cells transfected with scrambled RNA (shCTRL) were used as controls. The western blot quantification is presented as a grouped bar chart with error bars. Each bar represents the intensity means  $\pm$  s.d. of blots from three independent experiments.

A $\beta$ 25-35 treatment induced a decrease in PDIA3 protein levels of about 20%.

## RESULTS AND DISCUSSIONS

293T cells shPDIA3 were used as positive control. This result could suggest that the stress induced by A $\beta$ 25-35 causes the cell to trigger a defence that lead to a decrease in PDIA3 levels. To investigate whether this effect was due to a transcriptional regulation response, SH-SY5Y cells, treated with A $\beta$ 25-35 for 24 hours, were subjected to total RNA extraction, cDNA synthesis and qRT-PCR using specific primers to detect PDIA3 mRNA levels. Results obtained from qRT-PCR analysis are shown in the following figure:

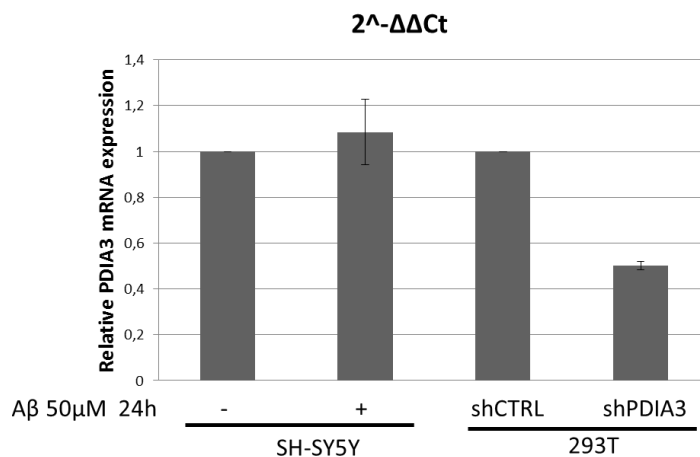


**Figure 18.** SH-SY5Y cells were treated with 50  $\mu$ M A $\beta$  for 24h. After total RNA extraction and cDNA synthesis, we performed a realtime PCR using proper primers to detect PDIA3 mRNA levels (see material and methods). 293T cells PDIA3 silenced (shPDIA3) and 293T cells transfected with scrambled RNA (shCTRL) were used as controls. The results presented here shows PDIA3 mRNA levels, normalized for  $\beta$ -actin, expressed in arbitrary units (AU). The results shown are the results of the average of three independent experiments.

Data shown in figure 18 indicates that the reduction in PDIA3 protein levels, observed in the western blot analysis, was not due to a decrease in mRNA levels. 293T shPDIA3 cells were used as positive control.

As further evidence, SH-SY5Y cells were treated with 50 $\mu$ M A $\beta$ 25-35 for 24 hours in presence or absence of 100  $\mu$ g/mL cyclohexamide.

## RESULTS AND DISCUSSIONS

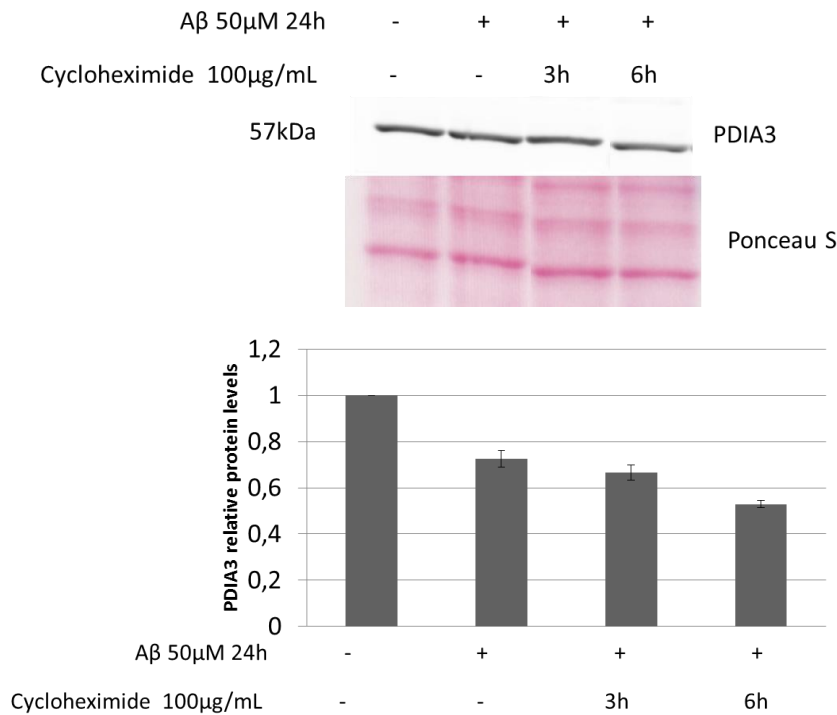


**Figure 19.** Proteins were extracted from SH-SY5Y cells after treatment with 50  $\mu$ M A $\beta$ 25-35 for 24hours in presence or absence of 100  $\mu$ g/mL cycloheximide, subjected to western blot analysis and revealed with anti-PDIA3 antibody. The western blot quantification is presented as a grouped bar chart with error bars. Each bar represents the intensity means  $\pm$  s.d. of blots from three independent experiments.

As shown in figure 19, when cells were treated for 6h with the protein synthesis inhibitor cycloheximide, the decrease in PDIA3 protein levels induced by A $\beta$  was more evident, going from 25% (A $\beta$  treatment) to 50% (A $\beta$ -cycloheximide co-treatment).

### ***4.2.2 The 25-35 fragment of the amyloid $\beta$ peptide does not induce ER stress in SH-SY5Y cells***

Since it has been reported that aggregates of A $\beta$  1-42 peptide induced ER

## RESULTS AND DISCUSSIONS

stress in neuronal cells [Chafekar et al., 2007; Lee et al., 2010], we wanted to verify if the decrease in PDIA3 levels could be a consequence of the UPR activation induced by A $\beta$ . To test that, SH-SY5Y cells were treated with A $\beta$  peptide for 24 hours and different UPR mediators were investigated. First, after cell lysis the expression levels of the ER chaperone BIP were analysed through western blot.

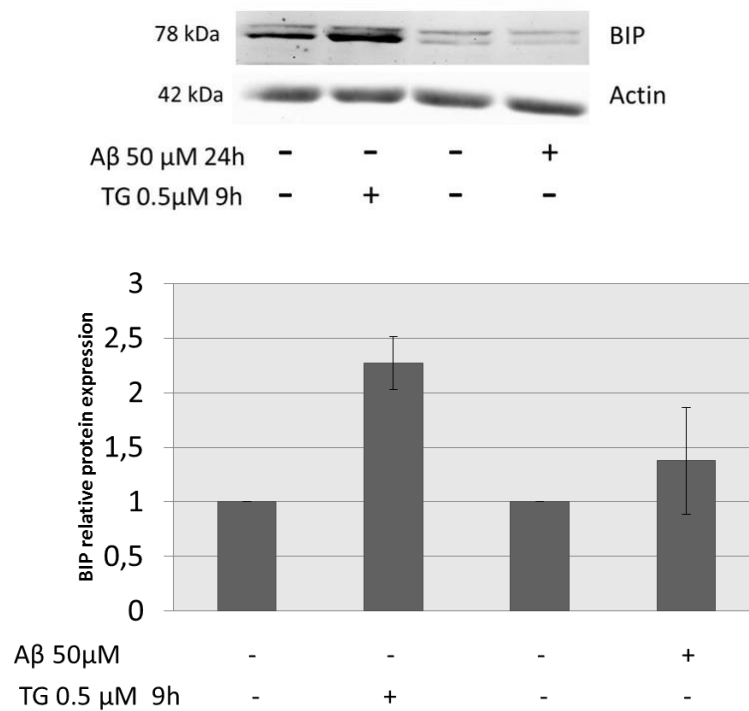


**Figure 20.** Proteins were extracted from SH-SY5Y cells after treatment with 50  $\mu$ M A $\beta$ 25-35 for 24h or Thapsigargin (TG) for 9h, subjected to western blot analysis and revealed with anti-BIP and anti-actin antibody. The western blot quantification is presented as a grouped bar chart with error bars. Each bar represents the intensity means  $\pm$  s.d. of blots from three independent experiments.

As noticeable in the figure above, there was no significant differences in BIP protein levels after 24 hours of treatment with A $\beta$  25-35. The ER stress

## RESULTS AND DISCUSSIONS

activator thapsigargin was used as a positive control.

Afterwards we analyzed the levels of the spliced form of XBP1, another UPR mediator, through RT-PCR, using a couple of primers which recognize both the spliced and unspliced form of XBP1.

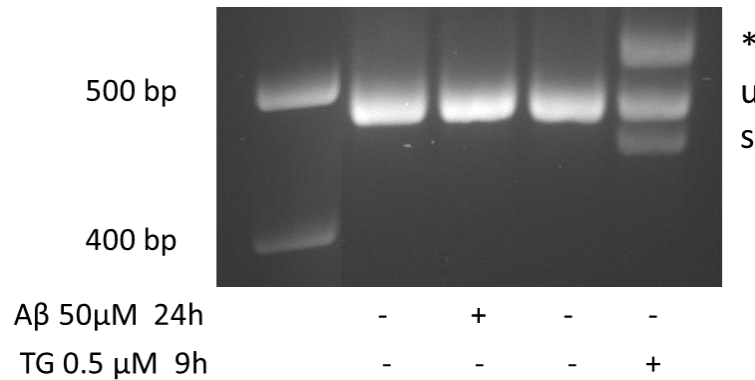


**Figure 21.** SH-SY5Y cells were treated with Aβ 50 μM for 24hours or thapsigargin (TG) 0.5 μM for 9 hours. After RNA extraction, Xbp-1mRNA splicing was determined by PCR. PCR products were separated by electrophoresis on 3% agarose gels. Products resulting from unspliced (“u”) an spliced (“s”) Xbp-1 mRNA are indicated. Asterisk identifies a hybrid amplicon resulting from spliced and unspliced Xbp-1 mRNA.

Aβ did not cause splicing of XBP1, as evident from the absence of the spliced form of XBP1 in the figure 21. Thapsigargin, on the other hand, caused ER stress and consequent activation of IRE1, which cleaves the XBP1 mRNA to obtain the active transcription factor represented by the spliced XBP1, indicated by the bottom band in figure 21.

To check if there was an earlier activation of UPR, SH-SY5Y cells were treated for 4 and 8 hours with amyloid β peptide and western blot analysis was performed to determine BIP levels.

## RESULTS AND DISCUSSIONS

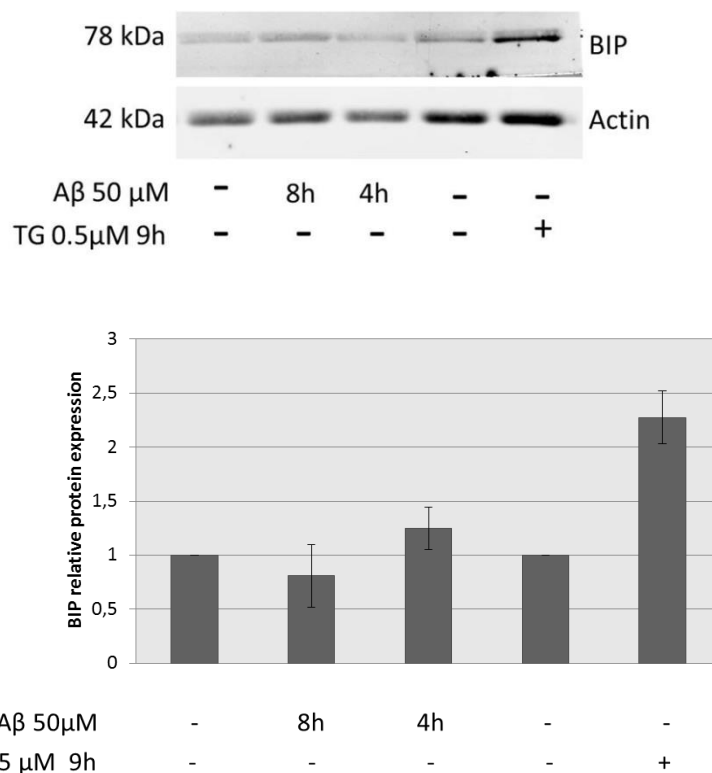


**Figure 22.** Proteins were extracted from SH-SY5Y cells after treatment with 50  $\mu$ M A $\beta$ 25-35 for 4 and 8 hours or Thapsigargin (TG) for 9hours, subjected to western blot analysis and revealed with anti-BIP and anti-actin antibody. The western blot quantification is presented as a grouped bar chart with error bars. Each bar represents the intensity means  $\pm$  s.d. of blots from three independent experiments.

As shown in figure 22, after 4 and 8 hours of treatment with A $\beta$ 25-35 there was no increase in BIP levels, suggesting that no UPR occurs after A $\beta$ -induced stress in SH-SY5Y cells. To further prove that there was no UPR activation, we also checked mRNA levels of CHOP and of the spliced form of XBP1 through RT-qPCR. As shown in figure 23, there was no increase in XBP1 spliced and CHOP mRNA levels after A $\beta$  treatment. All these data confirmed that the decrease in the PDIA3 levels, induced by A $\beta$  peptide treatment, was not due to ER stress and consequent UPR activation.

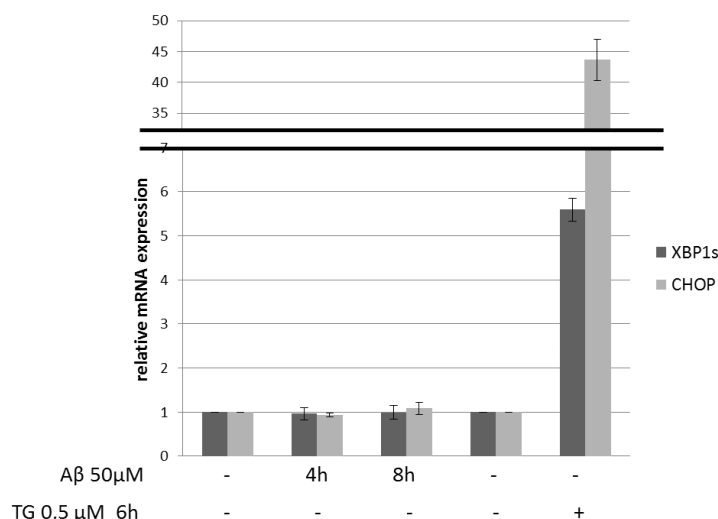


**Figure 23.** SH-SY5Y cells were treated with 50 μM Aβ for 4 and 8 hours and with 0.5 μM Thapsigargin (TG) for 6 hours as positive control. Untreated cells were used as a control. After total RNA extraction and cDNA synthesis, we performed a realtime PCR using proper primers to detect XBP1s, CHOP and β-actin mRNAs.

### *4.2.3 β-amyloid peptide treatment does not induce an PDIA3 degradation via proteasome in SH-SY5Y cells*

Given the results obtained, we hypothesized two possible scenarios as a cellular response to Aβ<sub>25-35</sub> treatment: PDIA3 protein degradation or secretion. To check if the decrease in PDIA3 protein levels under Aβ treatment was due to degradation dependent on the proteasome, the SH-SY5Y cell line was treated with Aβ in presence or absence of the specific proteasome inhibitor MG132. As shown in figure 24, there was no difference in PDIA3 proteins levels under Aβ treatment in presence or absence of MG132, meaning that the decrease in PDIA3 levels induced by Aβ peptide is not a consequence of the protein degradation through proteasome.

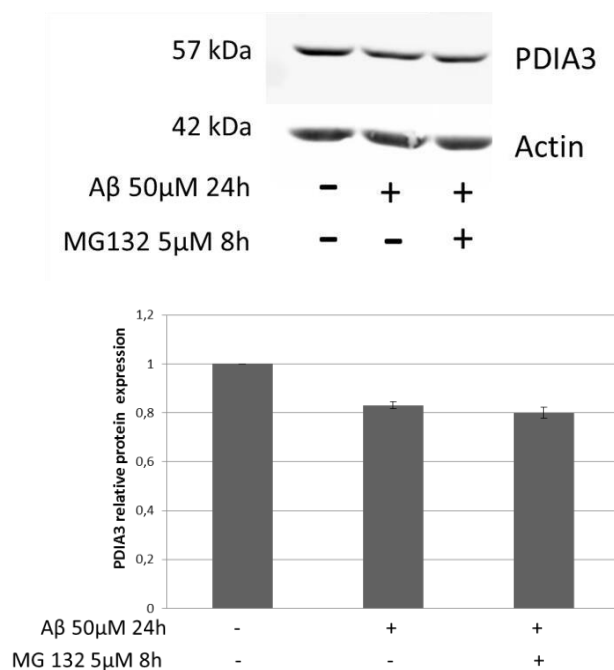


**Figure 24.** Proteins were extracted from SH-SY5Y cells after treatment with 50 μM Aβ<sub>25-35</sub> (Aβ) for 24hours in presence or absence of 5 μM MG132 (8 hours), subjected to western blot analysis and revealed with different antibodies: anti-PDIA3 (on the top) and anti-βactin (on the bottom). The western blot quantification is presented as a grouped bar chart with error bars. Each bar represents the intensity means ± s.d. of blots from three independent experiments.

#### *4.2.4 β-amyloid peptide treatment induces PDIA3 delocalization and secretion in SH-SY5Y cells*

Given the results obtained, the next step was to verify if the decrease in PDIA3 protein levels was due to secretion.

First of all, we analyzed PDIA3 subcellular localization under Aβ<sub>25-35</sub> treatment. SH-SY5Y cells were grown on microscope slides and treated with 50 μM Aβ<sub>25-35</sub> for 24 hours, cells were crosslinked with formaldehyde and permeabilized. Then we performed an immunostaining using an anti-PDIA3 antibody and a TRITC-conjugated secondary antibody. Nuclei were

## RESULTS AND DISCUSSIONS

visualized with DAPI staining. What obtained was then observed at a fluorescence microscope (Leica).

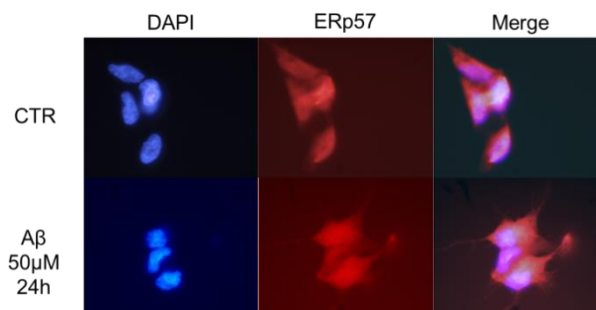


**Figure 25.** SH-SY5Y cells were grown on microscope slides, treated for 3, 6 and 24h with 50  $\mu$ M A $\beta$ 25-35, cross-linked with formaldehyde and permeabilized. Immunostaining was performed using anti-PDIA3 antibody and TRITC-conjugated secondary antibody. DAPI was used to stain nuclei. Cells were observed at a Leica fluorescence microscope.

From what is visible from figure 25, in the untreated sample (CTR), PDIA3 was mainly localized in the perinuclear region (compatible with ER localization), while it seems that after 24 hours,  $\beta$ -amyloid peptide induced PDIA3 delocalization toward the plasma membrane.

Considering these data, our hypothesis is that  $\beta$ -amyloid peptide could lead to PDIA3 translocation from the ER to the membrane surface and afterwards PDIA3 secretion in the extracellular space in order to counteract the toxic action of  $\beta$ -amyloid present in the culture medium. This is not the first evidence to show a possible PDIA3 secretion. Previous studies reported secretion of this ER resident protein even if it contains an ER retention signal [Hirano et al., 1995; Furie and Flaumenhaft, 2014; Dihazi et al., 2013]. Moreover this has been demonstrated for other ER chaperons [Genereux et al., 2015; Hahm et al., 2013; Obeid et al., 2007].

## RESULTS AND DISCUSSIONS

To test our hypothesis we treated SH-SY5Y cells with 50  $\mu$ M A $\beta$ 25-35 at different times and then subjected the culture media to Na-deoxycholate-TCA protein precipitation, acetone washing and proteins solubilization in SDS. Then we performed a western blot analysis using anti-PDIA3 antibody.

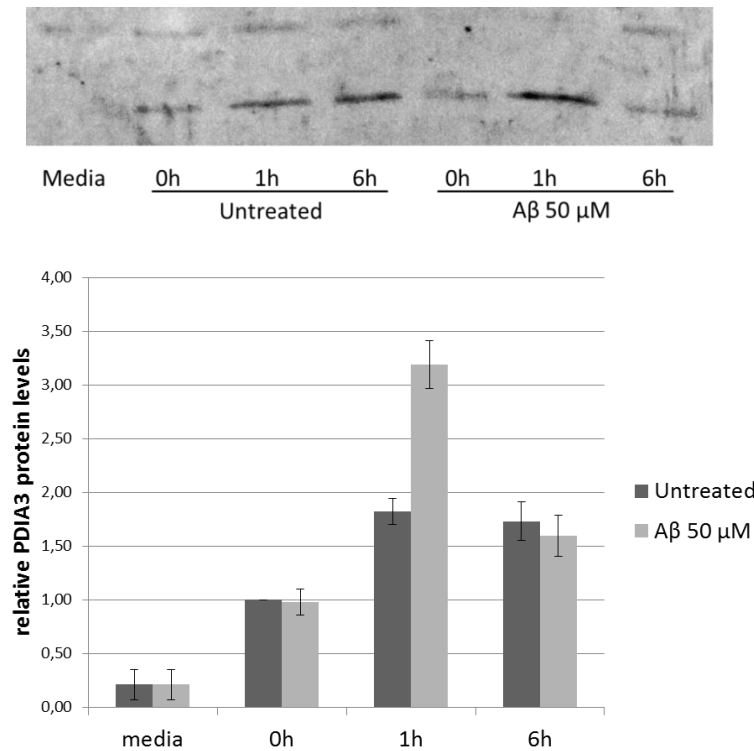


**Figure 26.** Secreted proteins from untreated (C) and A $\beta$ 25-35 treated (AB) SH-SY5Y cells were obtained subjecting culture media to Na-deoxycholate-TCA precipitation. Proteins were then analyzed by means of western blot using anti-PDIA3 antibody. The western blot quantification is presented as a grouped bar chart with error bars. Each bar represents the intensity means  $\pm$  s.d. of blots from three independent experiments.

The previous figure shows that SH-SY5Ys could secrete PDIA3 in absence of any treatment, but there was an increase in extracellular PDIA3 after treating cells with A $\beta$ 25-35 for one hour.

## RESULTS AND DISCUSSIONS

Furthermore, to check if PDIA3 was secreted through the canonical secretory pathway, SH-SY5Y cells were treated with A $\beta$  for 24h in presence or absence of the secretory trafficking inhibitor brefeldin A. Total proteins were extracted and subjected to western blot analysis to estimate PDIA3 levels.

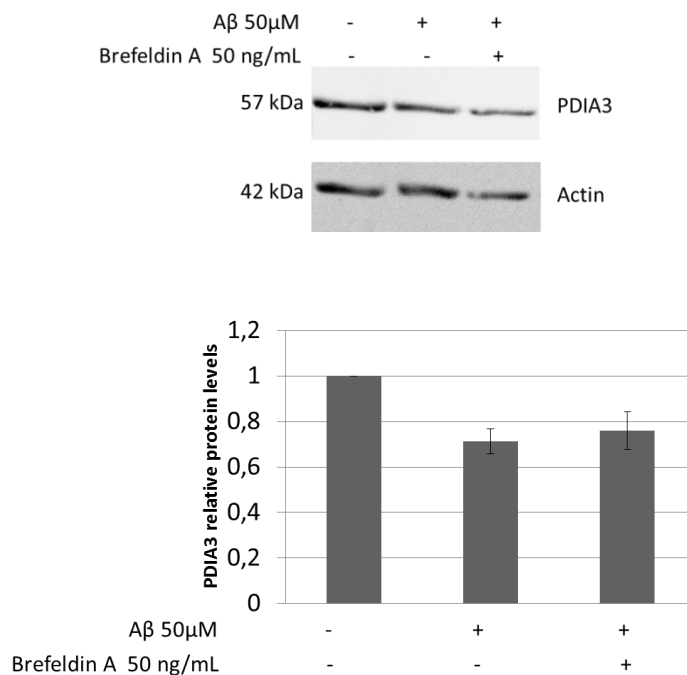


**Figure 27.** Proteins were extracted from SH-SY5Y cells after treatment with 50  $\mu$ M A $\beta$ 25-35 (A $\beta$ ) for 24hours in presence or absence of 50 ng/mL Brefeldin A (8 hours), subjected to western blot analysis and revealed with different antibodies: anti-PDIA3 (on the top) and anti- $\beta$ actin (on the bottom). The western blot quantification is presented as a grouped bar chart with error bars. Each bar represents the intensity means  $\pm$  s.d. of blots from three independent experiments.

From the results presented in figure 27, it is evident that brefeldin A did not rescue PDIA3 levels, meaning that this protein was not secreted through the canonical Golgi-mediated secretory pathway, under A $\beta$  treatment.

## RESULTS AND DISCUSSIONS

### 4.3 Discriminating between IRE1 activities

#### 4.3.1 *IRE1-GFP cleaves XBP1 mRNA and clusters in foci*

During my research activity at The Children's Hospital of Philadelphia, I focused my attention on the study of IRE1 activities. For this purpose we used the human haploid cell line, HAP1, knock-out for IRE1. First of all we checked the expression levels of IRE1 in HAP1 cells, both IRE1 +/+ and -/-, through western blotting analysis.

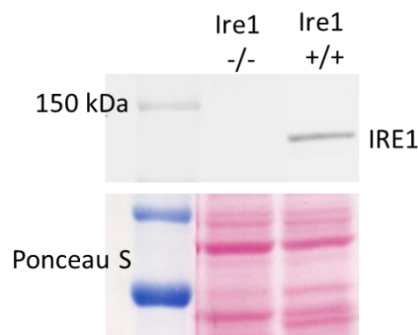


**Figure 28.** Proteins were extracted from HAP1 cells parental (IRE1+/+) and IRE1 KO (IRE1-/-), subjected to western blot analysis and revealed with anti IRE1 antibody.

As shown in the figure 28, the expression of IRE1 was completely abolished in the HAP1 IRE1 knock-out cells, while IRE1+/+ HAP1s showed a band around 110-120 kDa, corresponding to endogenous IRE1. In second place we assessed the IRE1 capability to cleave XBP1 mRNA through the splicing assay under ER stress. The figure 29 shows that HAP1 cells with endogenous IRE1 were able to cleave XBP1 mRNA in response to ER stress, as visible from the bottom band in the gel (s=spliced), while, as expected, IRE1 -/- HAP1s did not perform the XBP1 splicing.

## RESULTS AND DISCUSSIONS

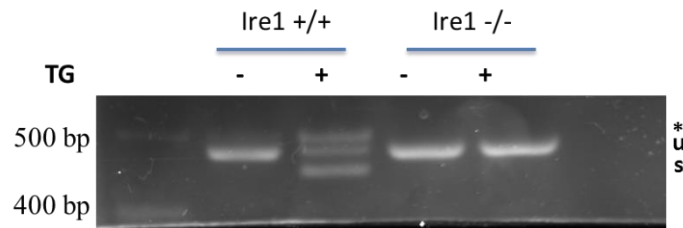


**Figure 29.** Parental (IRE1<sup>+/+</sup>) and IRE1 KO (IRE1<sup>-/-</sup>) HAP1 cells were treated with Thapsigargin 0.5  $\mu$ M for 4h. Total RNA was extracted and subjected to reverse transcription into cDNA. Xbp-1 mRNA splicing was determined by PCR. PCR products were separated by electrophoresis on 3% agarose gels. Products resulting from unspliced (“u”) and spliced (“s”) Xbp-1 mRNA are indicated. Asterisk identifies a hybrid amplicon resulting from spliced and unspliced Xbp-1 mRNA.

To begin studying IRE1 activities, a GFP-tagged fluorescent human IRE1 $\alpha$  fusion construct, IRE1-3-Flag-6-Histidine (3F6HGFP), with the fluorescent tag located in the non-conserved linker between the transmembrane domain and the kinase domain, was previously cloned in our lab (Fig. 30). The tag was placed in this area of the protein because in a previous study it was reported that yeast Ire1 tagged in the same position was functional, whereas the GFP tag in the C- or N-terminal abolished IRE1 functionality [Aragón et al., 2009].



**Figure 30.** Schematic representation of IRE1-GFP construct. LD=Luminal domain, TM=transmembrane domain, L=linker domain, K=kinase domain, R=endoribonuclease domain. 3F6H-GFP=inserted tag consisting of three FLAG epitopes followed by six histidines and a GFP. [Li et al., 2010]

We next established a stable IRE1<sup>-/-</sup> HAP1 cell line, in which the expression of WT-IRE1GFP and several point mutants was regulated through a doxycycline inducible system. Since it has been reported that, when IRE1 is

## RESULTS AND DISCUSSIONS

overexpressed, there is a spontaneous activation of its endoribonuclease domain, we first made sure not to induce IRE1 overexpression in our working conditions.. In this regard, IRE1<sup>-/-</sup> HAP1 cells, stably transduced with WT IRE1GFP and several point mutants, were treated with 1 $\mu$ g/mL of doxycycline for 24 hours to allow the expression of the recombinant protein. Total proteins were extracted and subjected to western blotting.

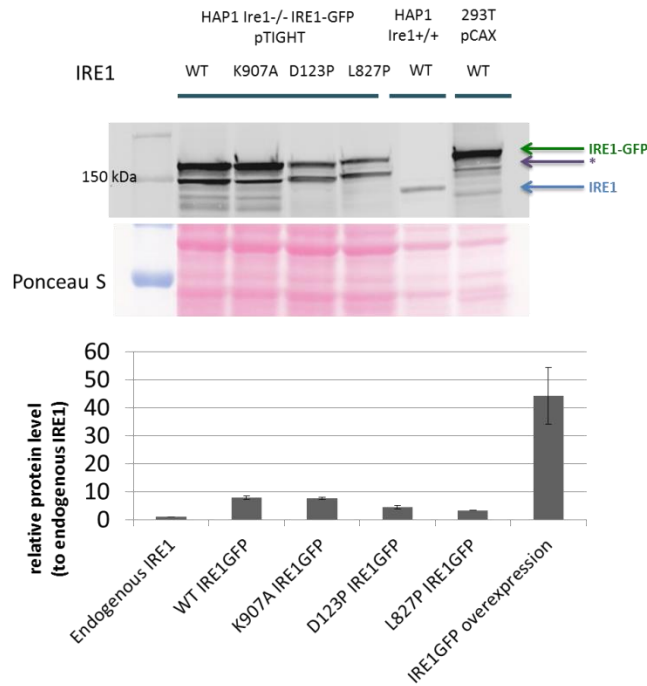


**Figure 31.** Proteins were extracted from HAP1 cells expressing endogenous IRE1 (IRE1<sup>+/+</sup>) and IRE1 KO (IRE1<sup>-/-</sup>) cells expressing WT-IRE1GFP and its mutants treated with 1 $\mu$ g/mL doxycycline, subjected to western blot analysis and revealed with anti IRE1 antibody. 293T cells transfected with pCAX-IRE1GFP were used as a model of IRE1 overexpression. The western blot quantification is presented as a grouped bar chart with error bars. Each bar represents the intensity means  $\pm$  s.d. of blots from three independent experiments.

As can be seen in figure 31, at the doxycycline concentration used, there was not overexpression of exogenous compared to the endogenous IRE1. On the other hand, IRE1 overexpression can be clearly observed in 293Ts

## RESULTS AND DISCUSSIONS

transfected with pCAX-IRE1GFP, which is a plasmid in which the expression of the protein of interest is under the control of a strong constitutive promoter. Once established that we were not working in overexpression conditions, we verified IRE1GFP ability to get activated in response to ER stress. After the expression of WT-IRE1GFP in IRE1<sup>-/-</sup> HAP1 cells, induced with 1 $\mu$ g/mL doxycycline, cells were treated with 0.2 $\mu$ M of the ER stress activator thapsigargin for different time points. Total RNA was extracted, subjected to reverse transcription into cDNA and PCR in order to detect the XBP1 mRNA splicing.

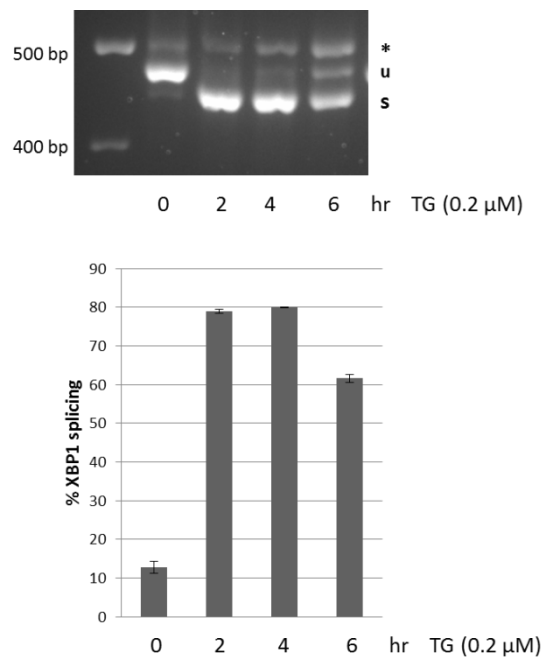


**Figure 32.** IRE1-GFP IRE1<sup>-/-</sup> HAP1s were treated with doxycycline (Dox) for 24h to induce IRE1GFP expression. After withdrawing of Dox, cells were treated with thapsigargin (TG) 0.2  $\mu$ M for different times. Xbp-1 mRNA splicing was determined by PCR. Products resulting from unspliced (“u”) and spliced (“s”) Xbp-1 mRNA are indicated. Asterisk identifies a hybrid amplicon resulting from spliced and unspliced Xbp-1 mRNA.

As shown in figure 32, IRE1GFP fusion protein restored splicing of XBP-1

## RESULTS AND DISCUSSIONS

mRNA in response to ER-stress. The next step was to evaluate the ability of IRE1GFP, under induction of ER stress with tunicamycin (Tm), to localize into discrete foci in the ER membrane.

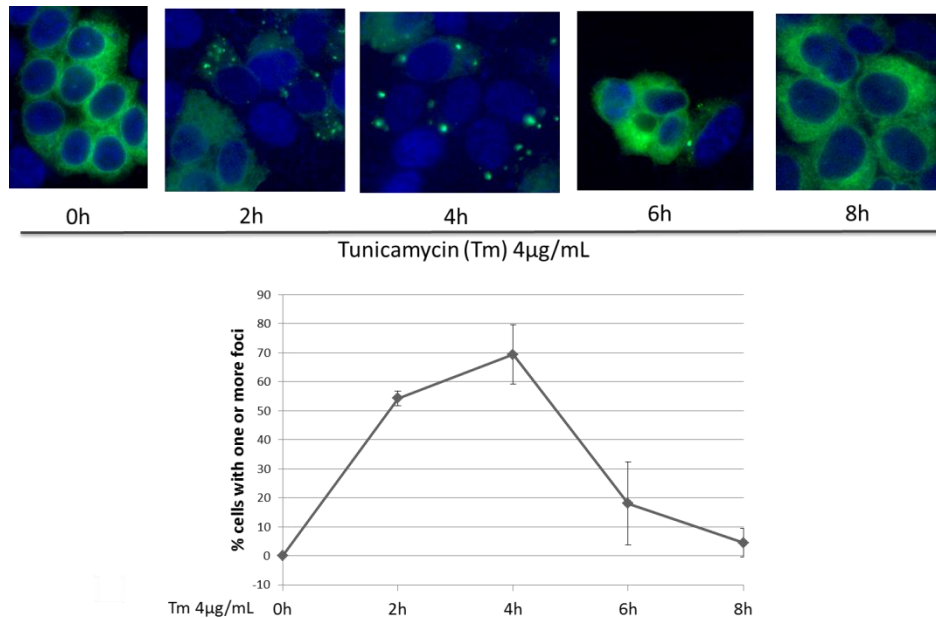


**Figure 33.** IRE1-GFP IRE1<sup>-/-</sup> HAP1s were treated with doxycycline (Dox) for 24h to induce IRE1GFP expression. At time 0, medium was replaced by medium containing no Dox but 4 μg/mL tunicamycin (Tm) to induce ER stress. IRE1GFP localization was evaluated over 8h time course. Percentage of cells with IRE1 foci was determined as quantification of time course experiment.

From figure 33, it appears that IRE1GFP clustered into many small foci after 2 h of Tm treatment. Upon persistent stress, these foci converted into fewer and larger ones and after 6 h of Tm treatment, we observed that IRE1 foci started to dissociate and completely resolved after 8 h. Moreover it was evident that a concomitant reappearance of fluorescence staining of the ER took place, suggesting a diffused redistribution of IRE1GFP over the ER membrane. These data suggest that the percentage of cells with IRE1 foci and

## RESULTS AND DISCUSSIONS

the Xbp-1 mRNA splicing follow a similar kinetic, with the maximum of activity after 2 and 4 hours. Furthermore, IRE1 activation was transitory even if the ER stress persisted.

### *4.3.2 An IRE1GFP defective luminal domain mutant is completely inactive*

The next step of our study was to evaluate the effects of a mutation in the luminal domain, which impairs IRE1 dimerization [Zhou et al., 2006], on IRE1 activities. In this respect, IRE1<sup>-/-</sup> HAP1 cells expressing D123P-IRE1GFP mutant, were treated with the ER stressor thapsigargin and XBP1 splicing assay was performed.

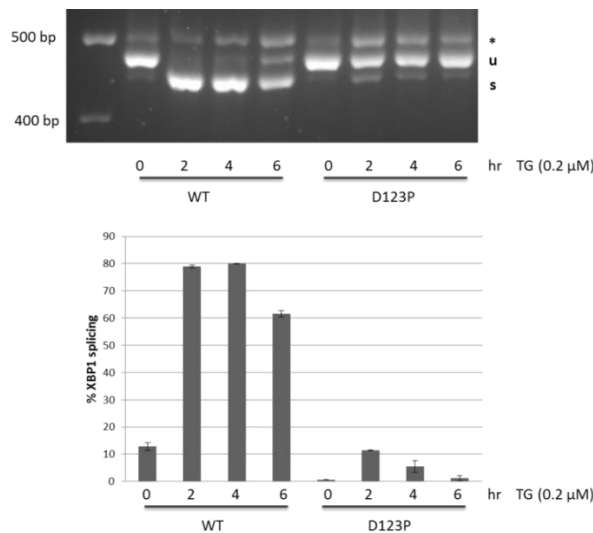


**Figure 34.** WT-IRE1GFP and D123P-IRE1GFP IRE1<sup>-/-</sup> HAP1s were treated with doxycycline (Dox) for 24h to induce IRE1GFP expression. After withdrawing of Dox, cells were treated with thapsigargin (TG) 0.2 μM for different times. Xbp-1mRNA splicing was determined by PCR. Products resulting from unspliced (“u”) an spliced (“s”) Xbp-1 mRNA are indicated. Asterisk identifies a hybrid amplicon resulting from spliced and unspliced Xbp-1 mRNA.

## RESULTS AND DISCUSSIONS

As can be observed in figure 34, the mutation of the aspartate 123 into a proline, impairing IRE1 dimerization, almost completely abolished IRE1 RNase activity, in comparison to WT-IRE1.

Next we investigated the ability of the D123P-IRE1GFP mutant to associate in clusters under ER stress.

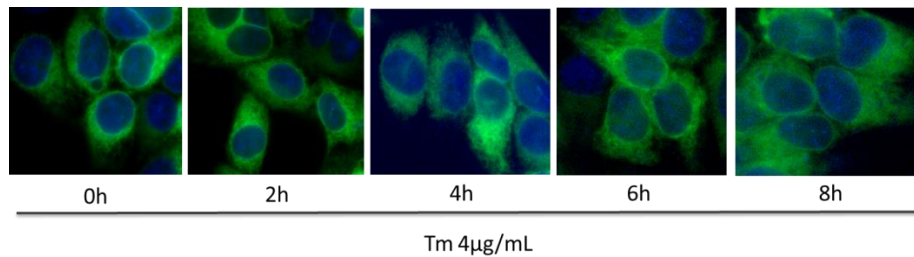


**Figure 35.** D123P-IRE1GFP IRE1<sup>-/-</sup> HAP1s were treated with doxycycline (Dox) for 24h to induce D123P-IRE1GFP expression. At time 0, medium was replaced by medium containing no Dox but 4 µg/mL tunicamycin (Tm) to induce ER stress. D123P-IRE1GFP localization was evaluated over 8h time course.

As can be seen in the figure above, the D123P mutant of IRE1, which is defective in self-association of the luminal domain, failed to cluster into foci upon tunicamycin treatment. From these data it was evident that a mutation in the luminal domain of IRE1, which impairs dimerization, caused a total suppression of IRE1 activity.

### ***4.3.3 An IRE1GFP defective endoribonuclease domain mutant does not cleave XBPI mRNA but clusters irreversibly into ER membrane***

For the next experiments we used an IRE1 mutant with a defective endoribonuclease domain [Tirasophon et al., 2000]. IRE1<sup>-/-</sup> HAP1 cells expressing K907A-IRE1GFP mutant, were treated with thapsigargin to induce ER stress and XBPI splicing assay was performed.

## RESULTS AND DISCUSSIONS

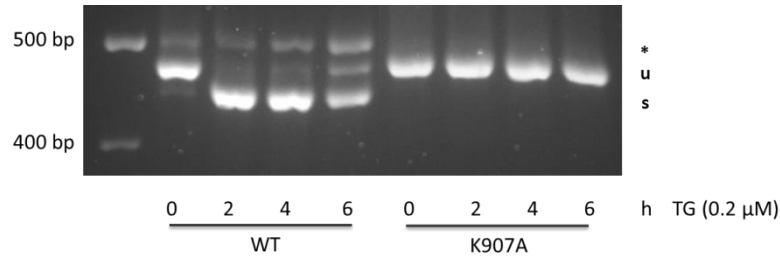


**Figure 36.** WT-IRE1GFP and K907A-IRE1GFP IRE1<sup>-/-</sup> HAP1s were treated with doxycycline (Dox) for 24h to induce IRE1GFP expression. After withdrawing of Dox, cells were treated with thapsigargin (TG) 0.2 μM for different times. Xbp-1 mRNA splicing was determined by PCR. Products resulting from unspliced (“u”) and spliced (“s”) Xbp-1 mRNA are indicated. Asterisk identifies a hybrid amplicon resulting from spliced and unspliced Xbp-1 mRNA.

As expected, the mutation of the lysine 907 into an alanine, which affects the RNase domain of IRE1, completely suppressed IRE1 capability to cleave the XBP1 mRNA. Further we evaluated the ability of this IRE1 mutant to relocalize into discrete foci in the ER membrane after induction of ER stress with tunicamycin. As shown in figure 37, K907A-IRE1GFP mutant clustered into big foci after 2 hours of tunicamycin treatment and it was evident that these big foci did not resolve over the time course experiment. This result was completely unexpected since from the data obtained from the WT protein it seemed that IRE1 clustering was related to its endoribonuclease activity. However the data obtained from this last experiment showed that IRE1 clustering is independent from its endoribonuclease activity and that IRE1 clustering initiation does not require a functional endoribonuclease domain. Moreover, a defect in this domain seemed to keep IRE1 in clusters over the time.

## RESULTS AND DISCUSSIONS

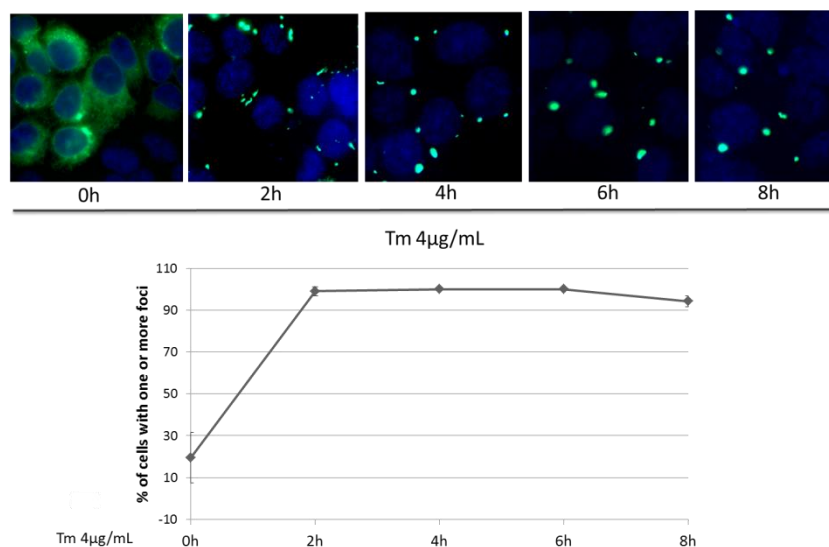


**Figure 37.** K907A-IRE1GFP IRE1<sup>-/-</sup> HAP1s were treated with doxycycline (Dox) for 24h to induce K907A-IRE1GFP expression. At time 0, medium was replaced by medium containing no Dox but 4 µg/mL tunicamycin (Tm) to induce ER stress. IRE1GFP localization was evaluated over 8h time course. Percentage of cells with IRE1 foci was determined as quantification of time course experiment.

To evaluate our hypothesis, we tested WT-IRE1GFP ability to associate in clusters under ER stress in presence of a known inhibitor of the RNase domain of IRE1, the small molecule 4µ8c [Cross et al.,2012]. As evident in figure 38, WT-IRE1GFP clustered into big foci after 2 hours of tunicamycin treatment in presence of the inhibitor 4µ8c and even in this case these big foci did not resolve over the time course experiment. 4µ8c is a small inhibitor which chemically interacts with the lysine 907 in the RNase domain of IRE1 leading to inhibition of both XBP1 splicing and RIDD activity [Cross et al., 2012].

## RESULTS AND DISCUSSIONS

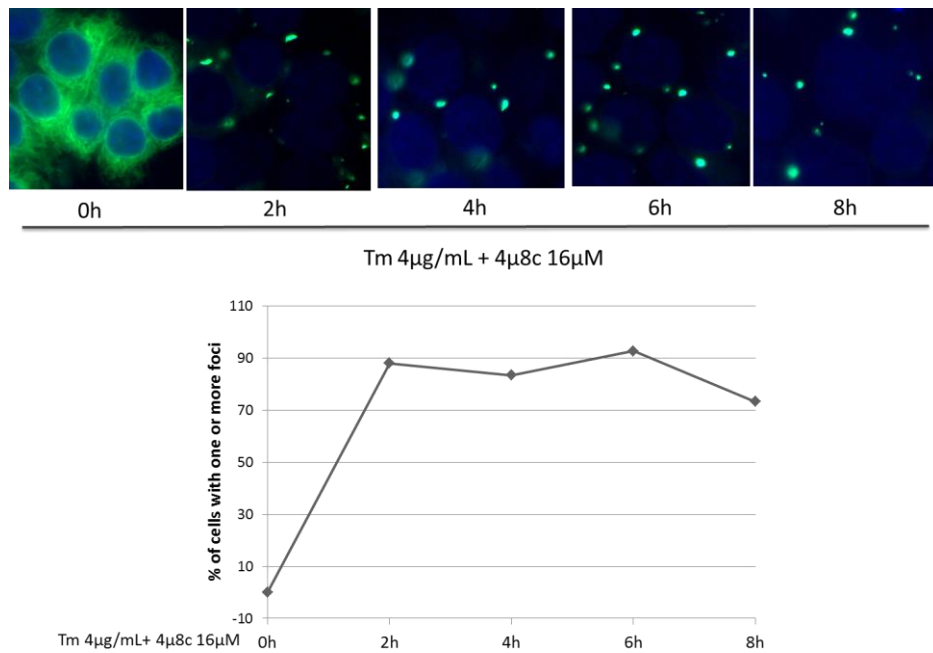


**Figure 38.** WT-IRE1GFP IRE1<sup>-/-</sup> HAP1s were treated with doxycycline (Dox) for 24h to induce IRE1GFP expression. At time 0, medium was replaced by medium containing no Dox but 4 µg/mL tunicamycin (Tm) and 16 µM 4µ8c. IRE1GFP localization was evaluated over 8h time course. Percentage of cells with IRE1 foci was determined as quantification of time course experiment.

Given these results, we can deduce that if the RNase domain of IRE1 is inhibited, either with a mutation (K907A) or using a small chemical inhibitor (4µ8c), IRE1 clusters in large foci in the ER membrane and these clusters do not resolve over the time. This could be explained by the existence of a negative feedback of the IRE1 RNase activity that could control IRE1 clustering. In this scenario, when the RNase domain of IRE1 is inhibited, there is no control on IRE1 clustering and therefore IRE1 persists in clusters. Another explanation could be that, when IRE1 cannot act as an endoribonuclease, it could perform other activities that could be related to its cluster state, for instance the activation of the JNK pathway. Given that IRE1

## RESULTS AND DISCUSSIONS

phosphorylation is a key event in IRE1 activation we also decided to test the phosphorylation state of the K907A mutant under ER stress. In this regard IRE1<sup>-/-</sup> HAP1 cells expressing K907A-IRE1GFP were treated with thapsigargin to induce ER stress for different time points. Total proteins were extracted and subjected to western blotting using anti IRE1 and phospho-IRE1 antibodies.

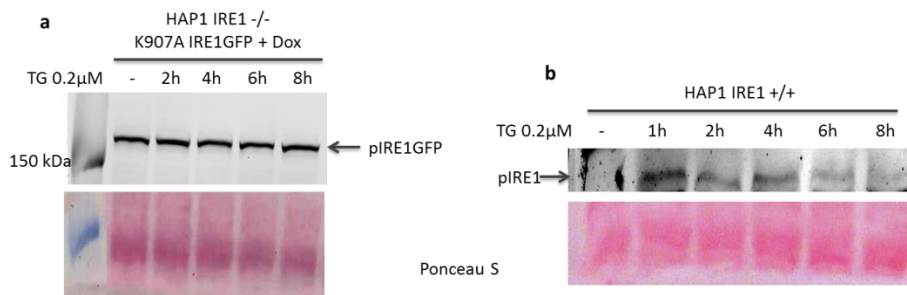


**Figure 39.** Proteins extracted from K907A-IRE1GFP IRE1<sup>-/-</sup> HAP1s, treated with increasing concentrations of doxycycline (Dox) for 24h to induce IRE1GFP expression and after that with thapsigargin (TG) 0.2 μM for 6 hours (a), and from IRE1<sup>+/+</sup> HAP1s treated with TG 0.2 μM for 6 hours (b), were subjected to western blot analysis and revealed with anti IRE1 and phospho-IRE1 antibodies.

As shown in the previous figure, the K907A mutant persisted in a phosphorylated state under ER stress; moreover it showed basal phosphorylation even without ER stress (Fig. 39a). This could explain why this mutant clustered spontaneously in absence of any ER stressor, even if in a limited percentage, 30% (Fig.37) vs. 0% in WT-IRE1 (Fig.33). Conversely WT-IRE1 was reversibly phosphorylated after thapsigargin treatment: after 8 hours of stress, IRE1 was completely dephosphorylated (Fig. 39b). As showed before in figure 33, WT IRE1 clusters resolved over the 8 hours treatment with thapsigargin. Considering all these data our hypothesis is that IRE1 ability to localize in foci within the ER membrane is strictly dependent

## RESULTS AND DISCUSSIONS

on its phosphorylation state.

### *4.3.4 The flavonoid luteolin induces XBP1 splicing acting from the cytosol but does not induce IRE1 clustering.*

Until this point we investigated IRE1 activities upon ER stress, which is known to induce BIP dissociation from the IRE1 luminal domain, its dimerization, trans-autophosphorylation, conformational changes and consequent activation of the RNase domain. The next step was to study IRE1 activities with a stimulus coming from the cytosol and not from the ER. To this end we used luteolin, a flavonoid which induces XBP1 splicing through direct binding to IRE1 at the interphase between the kinase and the endoribonuclease domain [Wiseman et al., 2010]. We treated IRE1<sup>+/+</sup> HAP1 cells with two concentrations of luteolin at different time points and performed the XBP1 mRNA splicing assay.

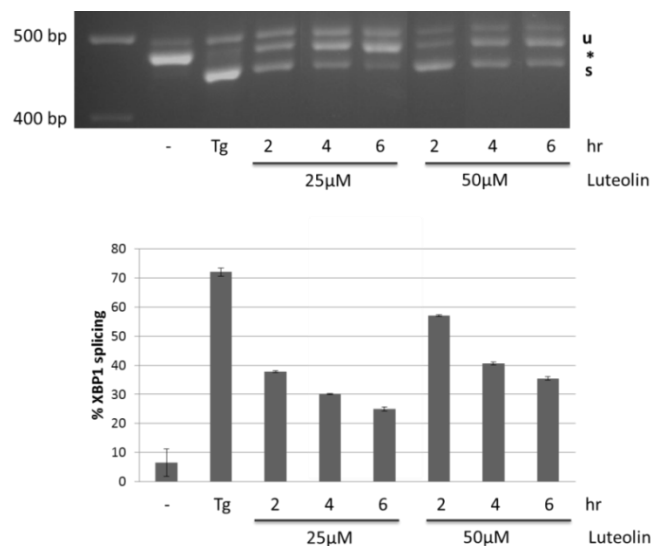


**Figure 40.** IRE1<sup>+/+</sup> HAP1 cells were treated with thapsigargin (TG) 0.2 μM for 6 hours or with two concentrations of luteolin for different times. Xbp-1mRNA splicing was

## RESULTS AND DISCUSSIONS

determined by PCR. Products resulting from unspliced (“u”) an spliced (“s”) Xbp-1 mRNA are indicated. Asterisk identifies a hybrid amplicon resulting from spliced and unspliced Xbp-1 mRNA.

As observed in the figure above, luteolin induced activation of the RNase domain of IRE1 in HAP1 cells. We then evaluated the ability of this flavonoid to cause localization of IRE1 into foci. To this end WT-IRE1GFP IRE1<sup>-/-</sup> HAP1 cells were treated with luteolin and IRE1GFP distribution was followed over the time.

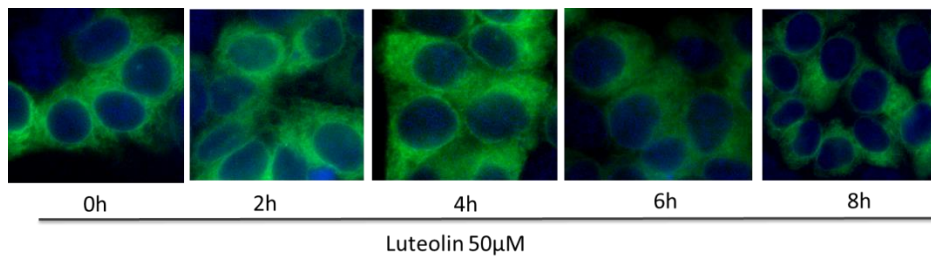


**Figure 41.** WT-IRE1GFP IRE1<sup>-/-</sup> HAP1s were treated with doxycycline (Dox) for 24h to induce IRE1GFP expression. At time 0, medium was replaced by medium containing no Dox but 50μM luteolin. IRE1GFP localization was evaluated over 8h time course.

As illustrated in the figure 41, luteolin did not cause IRE1 reorganization in clusters, even if it binds and activates IRE1 endoribonuclease domain. Considering these results and knowing that phosphorylation plays a pivotal role in IRE1 activation, we investigated the ability of luteolin to induce IRE1 phosphorylation. To this purpose IRE1<sup>+/+</sup> HAP1 cells were treated with luteolin at two different concentrations for 2 hours. Total proteins were extracted and subjected to western blotting using anti IRE1 and phospho-IRE1 antibodies.

## RESULTS AND DISCUSSIONS

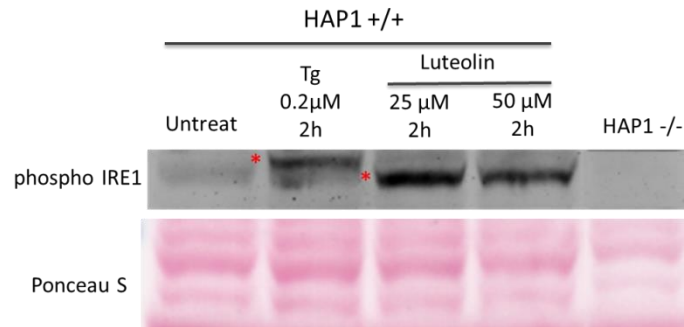


**Figure 42.** IRE1<sup>+/+</sup> HAP1s were treated with thapsigargin (TG) 0.2 μM for 2 hours or with two concentrations of luteolin for 2 hours. Proteins were extracted and subjected to western blot analysis and revealed with anti IRE1 and phospho-IRE1 antibodies.

From the figure 42 there is a significant shift between the band of phospho IRE1 under TG and under luteolin treatment. This could mean that luteolin induces a different degree in IRE1 phosphorylation. It is known from literature that IRE1 can be phosphorylated in different residues and that phosphorylation in the activation loop is sufficient to activate XBP1 splicing (Fig. 43) [Prischi et al., 2014].

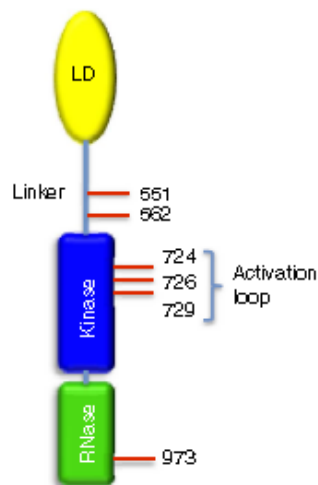


**Figure 43.** Position of phosphorylation sites in IRE1 structure (adapted from Prischi et al., 2014).

## RESULTS AND DISCUSSIONS

Therefore, we hypothesized that luteolin induces phosphorylation only in the IRE1 activation loop, leading to activation of its endoribonuclease domain and subsequent XBP1 splicing. Conversely IRE1 clustering could require phosphorylation in other residues. This could explain why luteolin did not induce IRE1 to localize into foci.

### 4.3.5 L827P IRE1-GFP is a fortuitous inactive mutant found in our lab.

When we first tried to recomplement IRE1<sup>-/-</sup> HAP1 cells with the doxycycline-inducible IRE1GFP, we performed the XBP1 mRNA splicing assay and surprisingly, as visible in the following figure, the exogenous IRE1 was not able to cleave the XBP1 mRNA.

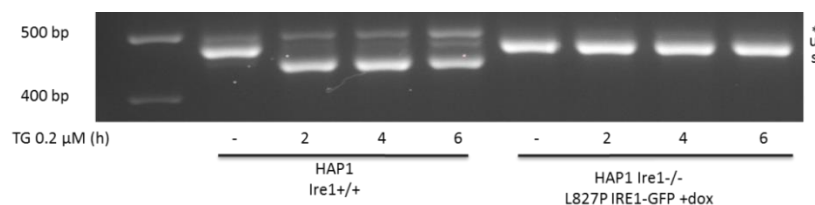


**Figure 44.** IRE1GFP IRE1<sup>-/-</sup> HAP1s were treated with doxycycline (Dox) for 24h to induce IRE1GFP expression. After withdrawing of Dox, cells were treated with thapsigargin (TG) 0.2 μM for different times. IRE1<sup>+/+</sup> HAP1 cells were used as positive control. Xbp-1 mRNA splicing was determined by PCR. Products resulting from unspliced (“u”) an spliced (“s”) Xbp-1 mRNA are indicated. Asterisk identifies a hybrid amplicon resulting from spliced and unspliced Xbp-1 mRNA.

This result was completely unexpected, since we knew from the literature [Li et al., 2010] and from other IRE1GFP plasmids present in our lab that IRE1 constructs with the GFP in the same position were completely active. In this respect we decided to sequence the whole IRE1GFP insert; what we found out was a single point mutation in a nucleotide which led to the mutation of the leucine in the position 827 into a proline.

## RESULTS AND DISCUSSIONS

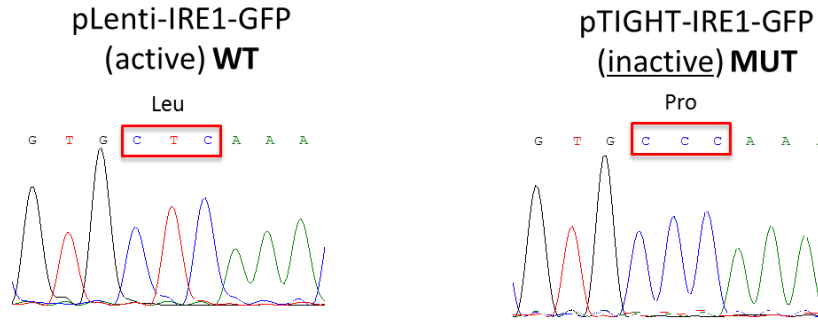


**Figure 45.** DNA sequencing of the pLenti-IRE1GFP (active) and pTIGHT-IRE1GFP (inactive) plasmids. The mutation led to the conversion of the CTC triplet, which encodes for Leucine 827 into a CCC triplet, which encodes for a proline. Mut, mutant type; Wt, wild-type.

This mutated residue is located between the kinase and the endoribonuclease domain of IRE1. The fact that a mutation not present in any of the catalytic domains of IRE1 led to the complete suppression of the IRE1 ability to cleave the XBP1 mRNA, encouraged us to investigate this new mutant of IRE1. To do that we followed the L827P IRE1GFP mutant localization in the ER membrane under ER stress over the time.

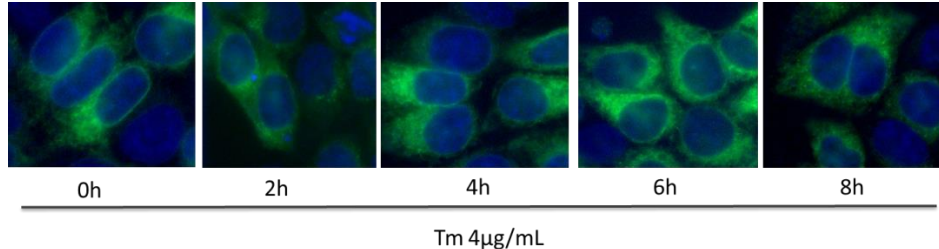


**Figure 46.** L827P-IRE1GFP IRE1<sup>-/-</sup> HAP1s were treated with doxycycline (Dox) for 24h to induce L827P-IRE1GFP expression. At time 0, medium was replaced by medium containing no Dox but 4 µg/mL tunicamycin (Tm) to induce ER stress. L827P-IRE1GFP localization was evaluated over 8h time course.

As shown in figure 46, this mutant did not cluster in foci under ER stress. So

## RESULTS AND DISCUSSIONS

this mutant seemed to behave like the D123P mutant, which is completely inactive, since it affects IRE1 dimerization. In order to understand if this new mutant was unable to dimerize, as the D123P, we decided to check its effect on endogenous IRE1. In this regard, IRE1<sup>+/+</sup> HAP1 cells, stably transduced with L827P-IRE1GFP mutant, were treated with increasing concentrations of doxycycline for 24 hours to allow the expression of the recombinant protein. The XBP1 mRNA splicing assay was performed under ER stress conditions.

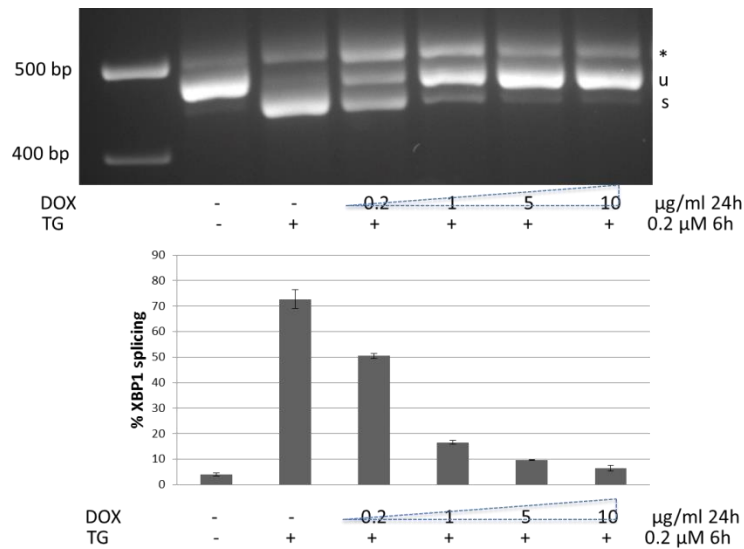


**Figure 47.** L827P-IRE1GFP IRE1<sup>+/+</sup> HAP1s were treated with increasing concentrations of doxycycline (Dox) for 24h to induce IRE1GFP expression. After withdrawing of Dox, cells were treated with thapsigargin (TG) 0.2  $\mu$ M for 6 hours. Xbp-1mRNA splicing was determined by PCR. Products resulting from unspliced (“u”) an spliced (“s”) Xbp-1 mRNA are indicated. Asterisk identifies a hybrid amplicon resulting from spliced and unspliced Xbp-1 mRNA.

As can be observed in figure 47, the L827P mutant inhibited endogenous IRE1 in a concentration-dependent manner, reaching an almost completely inhibition at concentrations of doxycycline between 5 and 10  $\mu$ g/mL. If this mutant can inhibit endogenous IRE1, we deduced that, differently from the

## RESULTS AND DISCUSSIONS

D123P, it is able to dimerize. At this point we decided to better characterize this inhibitory mutation. Since it is known that phosphorylation is important in IRE1 activation, the next step would be to check the phosphorylation state of this mutant. For some technical issues we were not able to investigate this aspect yet, but we checked the phosphorylation of endogenous IRE1 in presence of this mutant. IRE1<sup>+/+</sup> HAP1 cells, stably transduced with L827P-IRE1GFP mutant, were treated with increasing concentrations of doxycycline for 24 hours to allow the expression of the recombinant protein.

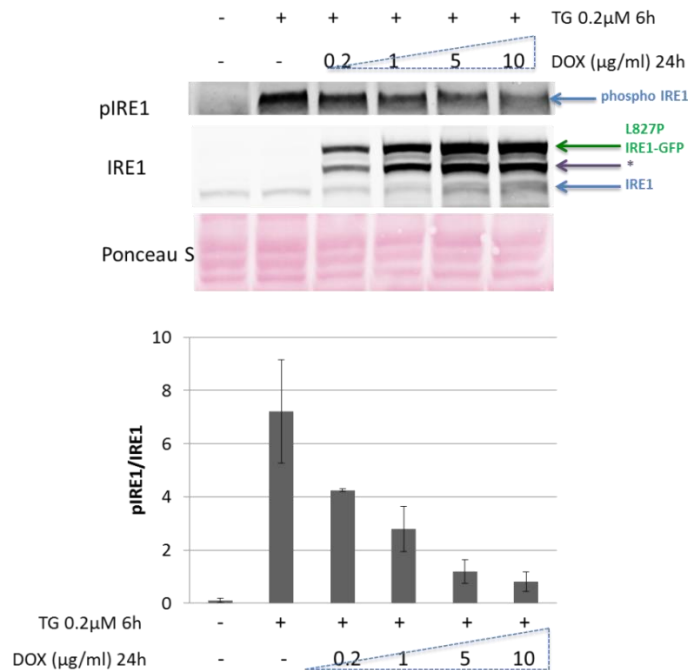


**Figure 48.** L827P-IRE1GFP IRE1<sup>+/+</sup> HAP1s were treated with increasing concentrations of doxycycline (Dox) for 24h to induce IRE1GFP expression. After withdrawing of Dox, cells were treated with thapsigargin (TG) 0.2 μM for 6 hours. Proteins were extracted and subjected to western blot analysis and revealed with anti IRE1 and phospho-IRE1 antibodies.

After treatment with thapsigargin for 6 hours to induce IRE1 phosphorylation, cells were lysed and total proteins were extracted and

## RESULTS AND DISCUSSIONS

subjected to western blotting using anti IRE1 and phospho-IRE1 antibodies. As shown in figure 48, the increase in the L827P mutant expression, achieved by increasing the doxycycline concentration, led to a decrease in the phosphorylation state of endogenous IRE1. These data suggest that this new mutant of IRE1 inhibits XBP1 splicing activity of IRE1 by inhibiting its phosphorylation. It is known from the literature that IRE1 phosphorylation causes conformational changes in the kinase and RNase domains of IRE1 necessary for IRE1 activation. As reported above, the flavonoid luteolin binds and activates XBP1 splicing activity of IRE1. The binding of this flavonoid occurs in the interphase between the kinase and endoribonuclease domains of IRE1 [Wiseman et al., 2010], the same region in which is located the L827P mutation. Knowing this, we decided to treat IRE1<sup>-/-</sup> HAP1 cells expressing the L827P-IRE1GFP with luteolin and to perform the XBP1 splicing assay.

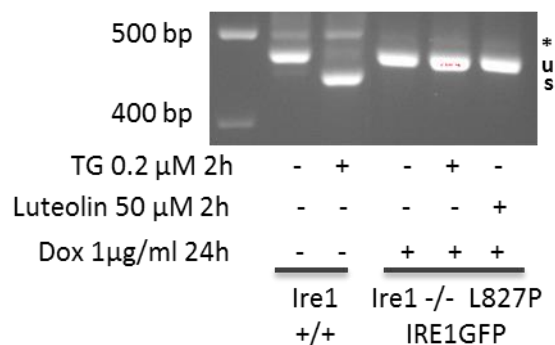


**Figure 49.** L827P IRE1GFP IRE1<sup>-/-</sup> HAP1s were treated with doxycycline (Dox) for 24h to induce L827P IRE1GFP expression. After withdrawing of Dox, cells were treated with thapsigargin (TG) 0.2 μM for different times. IRE1<sup>+/+</sup> HAP1 cells were used as positive control. Xbp-1 mRNA splicing was determined by PCR. Products resulting from unspliced (“u”) an spliced (“s”) Xbp-1 mRNA are indicated. Asterisk identifies a hybrid amplicon resulting from spliced and unspliced Xbp-1 mRNA.

From the figure above it was evident that luteolin did not rescue L827P

## RESULTS AND DISCUSSIONS

IRE1GFP ability to perform XBP1 splicing. As above reported, IRE1 activation requires its dimerization, phosphorylation and conformational changes which lead to juxtaposition of the RNase active sites of two adjacent protomers, orienting the relevant residues for catalysis (Fig 50a). Luteolin binds a pocket between the kinase and endoribonuclease domains of IRE1 and activates XBP1 splicing activity of IRE1 (Fig. 50b) [Wiseman et al., 2010]. In the case of the L827P mutant luteolin does not induce XBP1 splicing. We do not know yet if this result is due to the fact that luteolin cannot bind this mutant or if the binding occurs but the conformational changes required for activation are prevented (Fig. 50c). In both cases we think that the mutation of a leucine residue into a more rigid amino acid, such as proline, completely abolishes the ability of the RNase domain to reach the conformation required for its activity.

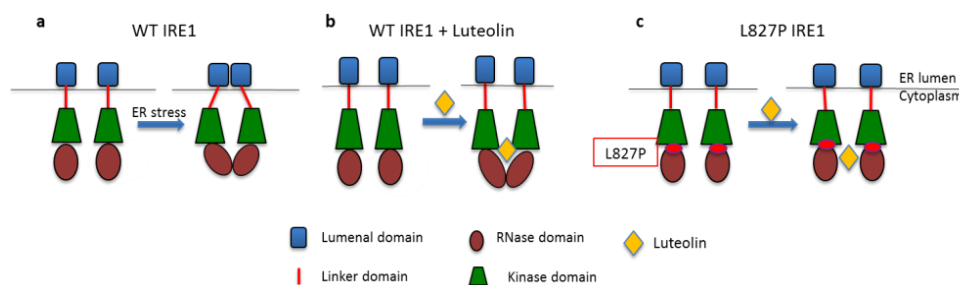


**Figure 50.** Schematic representation of IRE1 activation. WT-IRE1 in presence of ER stress dimerizes through its luminal domain and undergoes conformational changes that leads to RNase domain activation (a). Luteolin induces conformational changes without ER stress with consequent RNase domain activation in WT-IRE1 (b), but not in L827P-IRE1 (c).

## 5. CONCLUSIONS

In the first part of this study, the interaction of different flavonoids with PDIA3 and their effect on protein reductase activity were evaluated. Two molecules, eupatorin and eupatorin-5-methyl ether, showed the highest affinity for PDIA3 with a  $K_d$  near to  $1.0 \times 10^{-5}$  M. They also showed a noticeable inhibitory effect on disulphide reductase activity of PDIA3, but they did not significantly affect its DNA binding activity. The backbone structure of these two flavones is characterized by a more stable conformation where B and A rings are almost parallel (Fig. 13). This structure, associated with a definite degree of polarity, due to the presence of several methoxyl- groups, seems to be an important feature to determine a good affinity toward PDIA3. We can hypothesize that flavones interact with a region of the protein involving the tryptophan residues close to the redox site and given that PDIA3 does not contain any evident deep cavity or slot where this kind of ligands can bind, the binding of flavonoids may occur mainly via a flat interaction with the protein surface. Therefore, the planarity of the molecule as well as the number and specific position of its functional groups (hydroxyl-, methoxyl- and carbohydrates) will definitively play a major role to determine the affinity for the protein. In conclusion, eupatorin and eupatorin-5-methyl ether represent leading compounds for the binding to PDIA3 and for the inhibition of its redox activity. Further experiments are required to better characterize the effect of flavonoids on PDIA3 and to understand if some of the biological activities of these compounds are depending on the interaction with PDIA3. Since these flavones and PDIA3 are both involved in proliferative and carcinogenic processes, our in vitro findings on their interaction suggest that some of the biological effects of

## CONCLUSIONS

---

flavones could be mediated by modulation of PDIA3 activity. Additionally, this study will help to define and identify compounds to be used as selective inhibitors/modulators of PDIA3 biological activities.

Regarding the implications of PDIA3 in  $\beta$ -amyloid deposits and Alzheimer's disease, we observed that  $\beta$ -amyloid peptide fragment 25-35 induced a decrease in PDIA3 protein but not in mRNA levels. We demonstrated that this decrease was not a consequence of ER stress, since we proved that this specific fragment of the amyloid  $\beta$  peptide did not cause activation of the unfolded protein response. We also proved that this decrease was not due to protein degradation through proteasome. Moreover, we observed a delocalization of PDIA3 toward the plasma membrane following  $A\beta$  treatment. Considering our data and since evidences about PDIA3 extracellular presence can be found in the literature [Hirano et al., 1995; Erickson et al., 2005], we hypothesized that PDIA3 can be secreted under  $A\beta$  treatment. In this study we showed that PDIA3 is secreted by SH-SY5Y, with a significant increase after 1 hour of  $A\beta$ 25-35 treatment. We also observed that PDIA3 secretion seemed not to be dependent on the classical secretion pathway Golgi-mediated. An explanation for this observation could be that PDIA3 is released from the cell within exosomes. This is not totally unlikely since Marimpietri et al. found PDIA3 in exosomes coming from a neuroblastoma cell line [Marimpietri et al., 2013]. Moreover PDIA3 is present in the ExoCarta Database as an exosome-associated protein. From data presented in this work, our hypothesis is that  $\beta$ -amyloid peptide induces a PDIA3 delocalization and secretion in the extracellular fluid as a possible defence mechanism carried out by the cell to counteract the toxic action of  $A\beta$ . Considering the work of Erickson et al., it could be that PDIA3 pursues

this aim through direct binding to amyloid  $\beta$  peptide in order to prevent its aggregation and keep it in solution.

In the last part of my PhD, I focused my attention on ER stress and Unfolded Protein Response, in particular on one of its sensors, IRE1. The main focus was to study IRE1 activities, with special regard to the involvement of IRE1 domains in its activation. We were also interested in how IRE1 clusters are related to its activities and how phosphorylation regulates them. In this study we observed that, in order to have activation of the RNase domain of IRE1 and clustering, a functional luminal domain is required. Interestingly we found out that if the RNase domain of IRE1 is somehow inhibited, with a mutation or using a chemical inhibitor, IRE1 persists in clusters in the ER membrane. This means that IRE1 clustering initiation does not require the endoribonuclease activity of IRE1. Moreover this led us to hypothesize that IRE1 clustering can be related to other activities, such as RIDD or activation of the JNK pathway. Another interesting finding in this study was that a stimulus coming from the cytosol induces XBP1 mRNA splicing but not IRE1 clustering. Indeed, the flavonoid luteolin, through direct binding to the interphase between the kinase and endoribonuclease domains, triggers the splicing of XBP1 mRNA but it does not cause IRE1 redistribution in clusters in the ER membrane. This could be explained by the finding that luteolin induces a different degree in IRE1 phosphorylation if compared with the one induced by a common ER stress activator, such as thapsigargin. Our hypothesis is that luteolin induces phosphorylation only in the activation loop, which is sufficient to have XBP1 splicing, as proved by Prischi et al [Prischi et al., 2014], but in order to have IRE1 clustering, phosphorylation in additional residues is required. More studies are needed to confirm our

## CONCLUSIONS

---

hypothesis and, more importantly, the next step will be to investigate the other IRE1 activities, RIDD and JNK-pathway activation, in order to relate every single IRE1 activity to its dimeric or oligomeric state. Moreover we want to better understand how the phosphorylation state of IRE1 affects its activities. Last, during the course of this study on IRE1, we discovered by chance a new IRE1 mutant, L827P, which has proven to be also an inhibitor of this enzyme. We are now interested in better characterizing the mechanism of action of this mutant with the intent to develop, in the future, small peptides that can inhibit IRE1 activity. Since it has been proved that IRE1 is involved in different pathologies, such as multiple myeloma, it can be used as a valid and promising pharmacological target.

## REFERENCES

- Adikesavan AK, Unni E, Jaiswal AK. Overlapping signal sequences control nuclear localization and endoplasmic reticulum retention of GRP58. *Biochem Biophys Res Commun.* 2008, 377(2): 407-12.
- Ali MM, Bagratuni T, Davenport EL, Nowak PR, Silva-Santisteban MC, Hardcastle A, McAndrews C, Rowlands MG, Morgan GJ, Aherne W, Collins I, Davies FE, Pearl LH. Structure of the Ire1 autophosphorylation complex and implications for the unfolded protein response. *EMBO J.* 2011, 30: 894–905.
- Altieri F, Maras B, Eufemi M, Ferraro A, Turano C. Purification of a 57kDa nuclear matrix protein associated with thiol:protein-disulfide oxidoreductase and phospholipase C activities. *Biochem. Biophys. Res. Commun.* 1993, 194: 992-1000.
- Aragón T, van Anken E, Pincus D, Serafimova IM, Korennykh AV, Rubio CA, Walter P. Messenger RNA targeting to endoplasmic reticulum stress signalling sites. *Nature.* 2009, 457(7230): 736-40.
- Atherton E, Sheppard RC. Solid Phase Synthesis – A Practical Approach. IRL Press at Oxford University Press, USA. 1989 p. 203.
- Aune D, Chan DS, Vieira AR, Rosenblatt DA, Vieira R, Greenwood DC, Norat T. Fruits, vegetables and breast cancer risk: a systematic review and meta-analysis of prospective studies. *Breast Cancer Res Treat.* 2012, 134: 479–93.
- Bertolotti A, Zhang Y, Hendershot L, Harding H, Ron D. Dynamic interaction of BiP and the ER stress transducers in the unfolded protein response. *Nat Cell Biol.* 2000, 2: 326–332.
- Bi S, Song D, Tian Y, Zhou X, Liu Z and Zhang H. Molecular spectroscopic study on the interaction of tetracyclines with serum albumins. *Spectrochim Acta A Mol Biomol Spectrosc.* 2005, 61(4): 629-36.
- Blennow K, de Leon MJ, Zetterberg H. Alzheimer's disease. *Lancet* 2006, 368 (9533): 387–403.
- Boyan BD, Chen J, Schwartz Z. Mechanism of Pdia3-dependent 1 $\alpha$ ,25-dihydroxy vitamin D3 signaling in musculoskeletal cells. *Steroids.* 2012, 77(10): 892-6.
- Boyce M, Bryant KF, Jousse C, Long K, Harding HP, Scheuner D, Kaufman RJ, Ma D, Coen DM, Ron D, Yuan J. A selective inhibitor of eIF2 $\alpha$  dephosphorylation protects cells from ER stress. *Science.* 2005, 307: 935–939.
- Bravo L. Polyphenols: chemistry, dietary sources, metabolism, and nutritional significance. *Nutr Rev.* 1998, 56: 317–333.

- Breckenridge DG, Germain M, Mathai JP, Nguyen M, Shore GC. Regulation of apoptosis by endoplasmic reticulum pathways. *Oncogene*. 2003, 22: 8608–18.
- Calfon M, Zeng H, Urano F, Till JH, Hubbard SR, Harding HP, Clark SG, Ron D. IRE1 couples endoplasmic reticulum load to secretory capacity by processing the XBP-1 mRNA. *Nature*. 2002, 415: 92–96.
- Cao SS, and Kaufman RJ. Unfolded protein response. *Curr. Biol*. 2012, 22: R622-R626.
- Carvalho AT, Fernandes PA, Swart M, Van Stralen JN, Bickelhaupt FM, Ramos MJ. Role of the variable active site residues in the function of thioredoxin family oxidoreductases. *J Comput Chem*. 2009, 30(5): 710-24.
- Chafekar SM, Hoozemans JJ, Zwart R, Baas F, Scheper W. Abeta 1-42 induces mild endoplasmic reticulum stress in an aggregation state-dependent manner. *Antioxid Redox Signal*. 2007, 9: 2245–2254.
- Cheng Z, Zhang J, Ballou DP, Williams CH Jr. Reactivity of thioredoxin as a protein thiol-disulfide oxidoreductase. *Chem Rev*. 2011, 14;111(9): 5768-83.
- Chichiarelli S, Ferraro A, Altieri F, Eufemi M, Coppari S, Grillo C, Arcangeli V, Turano C. The stress protein PDIA3/GRP58 binds specific DNA sequences in HeLa cells. *J. Cell. Physiol*. 2007, 210: 343-351.
- Chichiarelli S, Gaucci E, Ferraro A, Grillo C, Altieri F, Cocchiola R, Arcangeli V, Turano C, Eufemi M. Role of PDIA3 in the signaling and transcriptional activity of STAT3 in a melanoma cell line. *Archives of biochemistry and biophysics*. 2010, 494: 178-183.
- Coe H, Jung J, Groenendyk J, Prins D, Michalak M. PDIA3 modulates STAT3 signaling from the lumen of the endoplasmic reticulum. *The Journal of biological chemistry*. 2010, 285: 6725-6738.
- Coelho DS, Cairrao F, Zeng X, Pires E, Coelho AV, Ron D, Ryoo HD, and Domingos PM. Xbp1-independent Ire1 signaling is required for photoreceptor differentiation and rhabdomere morphogenesis in *Drosophila*. *Cell Rep*. 2013, 5: 791–801.
- Coelho DS, Domingos PM. Physiological roles of regulated Ire1 dependent decay. *Front Genet*. 2014, 5: 76.
- Coppari S, Altieri F, Ferraro A, Chichiarelli S, Eufemi M, Turano C. Nuclear localization and DNA interaction of protein disulfide isomerase PDIA3 in mammalian cells. *J Cell Biochem*. 2002, 85 (2): 325-333.
- Credle JJ, Finer-Moore JS, Papa FR, Stroud RM, Walter P. On the mechanism of

- sensing unfolded protein in the endoplasmic reticulum. *Proc Natl Acad Sci.* 2005, 102: 18773–18784.
- Cross BC, Bond PJ, Sadowski PG, Jha BK, Zak J, Goodman JM, Silverman RH, Neubert TA, Baxendale IR, Ron D, Harding HP. The molecular basis for selective inhibition of unconventional mRNA splicing by an IRE1-binding small molecule. *Proc Natl Acad Sci.* 2012, 109(15): E869-78.
- Davies MP, Barraclough DL, Stewart C, Joyce KA, Eccles RM, Barraclough R, Rudland PS, Sibson DR. Expression and splicing of the unfolded protein response gene XBP-1 are significantly associated with clinical outcome of endocrine-treated breast cancer. *Int J Cancer.* 2008, 123: 85– 88.
- Dick TP, Bangia N, Peaper DR, Cresswell P. Disulfide bond isomerization and the assembly of MHC class I-peptide complexes. *Immunity.* 2002, 16: 87-98.
- Dihazi H, Dihazi GH, Bibi A, Eltoweissy M, Mueller CA, Asif AR, Rubel D, Vasko R, Mueller GA. Secretion of PDIA3 is important for extracellular matrix accumulation and progression of renal fibrosis, and is an early sign of disease onset. *J Cell Sci.* 2013, 126(16): 3649-63.
- Dihazi H, Dihazi GH, Jahn O, Meyer S, Nolte J, Asif AR, Mueller GA, Engel W. Multipotent adult germline stem cells and embryonic stem cells functional proteomics revealed an important role of eukaryotic initiation factor 5A (Eif5a) in stem cell differentiation. *J. Proteome Res.* 2011, 10: 1962-1973.
- Dong G, Wearsch PA, Peaper DR, Cresswell P, Reinisch KM. Insights into MHC class I peptide loading from the structure of the tapasin-PDIA3 thioloxydoreductase heterodimer. *Immunity.* 2009, 30: 21-32.
- Ellerman DA, Myles DG, Primakoff P. A role for sperm surface protein disulfide isomerase activity in gamete fusion: evidence for the participation of PDIA3. *Dev. Cell.* 2006, 10: 831-837.
- Ellgaard, L., Ruddock, L. W. The human protein disulphide isomerase family: substrate interactions and functional properties. *EMBO Rep.* 2005; 6(1):28-32.
- Engin F, Yermalovich A, Nguyen T, Hummasti S, Fu W, Eizirik DL, Mathis D, Hotamisligil GS. Restoration of the unfolded protein response in pancreatic  $\beta$  cells protects mice against type 1 diabetes. *Sci Transl Med.* 2013, 5(211): 211ra156.
- Erickson RR, Dunning LM, Holtzman JL. The effect of aging on the chaperone concentrations in the hepatic, endoplasmic reticulum of male rats: the possible role of protein misfolding due to the loss of chaperones in the decline in physiological function seen with age. *J. Gerontol.Biol.Med.* 2006, 61A: 435–443.
- Erickson RR, Dunning LM, Olson DA, Cohen SJ, Davis AT, Wood WG, Kratzke

- RA, Holtzman JL. In cerebrospinal fluid ER chaperones PDIA3 and calreticulin bind beta-amyloid. *Biochem Biophys Res Commun.* 2005, 332: 50–7.
- Eufemi M, Coppari S, Altieri F, Grillo C, Ferraro A, Turano C. PDIA3 is present in STAT3-DNA complexes. *Biochemical and biophysical research communications.* 2004, 323: 1306-1312.
- Ferrari DM, Söling HD. The protein disulphide-isomerase family: unravelling a string of folds. *Biochem J.* 1999; 339 ( Pt 1):1-10.
- Ferraro A, Altieri F, Coppari S, Eufemi M, Chichiarelli S, Turano C. Binding of the protein disulfide isomerase isoform ERp60 to the nuclear matrix-associated regions of DNA. *J. Cell. Biochem.* 1999, 72: 528-539.
- Frank DA. Transcription factor STAT3 as a prognostic marker and therapeutic target in cancer. *Journal of clinical oncology : official journal of the American Society of Clinical Oncology.* 2013, 31: 4560-4561.
- Furie B, Flaumenhaft R. Thiol isomerases in thrombus formation. *Circ Res.* 2014, 114(7): 1162-73.
- Garbi N, Tanaka S, Momburg F, Hammerling G.J. Impaired assembly of the major histocompatibility complex class I peptide-loading complex in mice deficient in the oxidoreductase PDIA3. *Nat. Immunol.* 2006. 7: 93-102.
- Genereux JC, Qu S, Zhou M, Ryno LM, Wang S, Shoulders MD, Kaufman RJ, Lasmézas CI, Kelly JW, Wiseman RL. Unfolded protein response-induced ERdj3 secretion links ER stress to extracellular proteostasis. *EMBO J.* 2015, 34(1): 4-19.
- George VC, Vijesh VV, Dehigaspege AI, Lakshmi CA, Anbarasu K, Kumar DR, Ethiraj R, Kumar RA, Rupasinghe HP. Mechanism of Action of Flavonoids in Prevention of Inflammation-Associated Skin Cancer. *Curr Med Chem.* 2016 Jun 27. [Epub ahead of print]
- Gonzalez TN, Sidrauski C, Dörfler S, Walter P. Mechanism of non-spliceosomal mRNA splicing in the unfolded protein response pathway. *EMBO J.* 1999, 18: 3119–3132.
- Grillo C, Coppari S, Turano C, Altieri F. The DNA-binding activity of protein disulfide isomerase PDIA3 is associated with the a(′) domain. *Biochem Biophys Res Commun.* 2002, 295(1): 67-73.
- Grillo C, D'Ambrosio C, Consalvi V, Chiaraluce R, Scaloni A, Maceroni M, Eufemi M, Altieri F. DNA-binding activity of the PDIA3 C-terminal domain is related to a redox-dependent conformational change. *J. Biol. Chem.* 2007, 282: 10299-10310.
- Grillo C, D'Ambrosio C, Scaloni A, Maceroni M, Merluzzi S, Turano C, Altieri F.

- Cooperative activity of Ref-1/APE and PDIA3 in reductive activation of transcription factors. *Free radical biology & medicine*. 2006, 41(7): 1113-1123.
- Hahm E, Li J, Kim K, Huh S, Rogelj S, Cho J. Extracellular protein disulfide isomerase regulates ligand-binding activity of alphaMbeta2 integrin and neutrophil recruitment during vascular inflammation. *Blood*. 2013, 121: 3789-3800.
- Halliwell B. Oxidative stress and neurodegeneration: where are we now? *J Neurochem*. 2006, 97(6): 1634-58.
- Halperin L, Jung J, and Michalak M. The many functions of the endoplasmic reticulum chaperones and folding enzymes. *IUBMB Life*. 2014, 66: 318–326.
- Han D, Lerner AG, Vande Walle L, Upton JP, Xu W, Hagen A, Backes BJ, Oakes SA, Papa FR. IRE1alpha kinase activation modes control alternate endoribonuclease outputs to determine divergent cell fates. *Cell*. 2009, 138: 562–575.
- Hatahet F, Ruddock LW: Protein disulfide isomerase. a critical evaluation of its function in disulfide bond formation. *Antioxid Redox Signal*. 2009, 11(11): 2807-50.
- Hertog MGL, Fesens EJM, Hollman PCH, Katan MB, Kromhout D. Dietary antioxidant flavonoids and the risk of coronary heart disease: The Zutphen elderly study. *Lancet* . 1993, 342: 1007-1011.
- Hetz C and Glimcher LH. Protein homeostasis networks in physiology and disease. *Curr. Opin. Cell Biol*. 2011, 23: 123–125.
- Hetz C, and Mollereau B. Disturbance of endoplasmic reticulum proteostasis in neurodegenerative diseases. *Nat.Rev. Neurosci*. 2014, 15: 233–249.
- Hetz C, Martinon F, Rodriguez D, Glimcher LH. The unfolded protein response: integrating stress signals through the stress sensor IRE1alpha. *Physiol. Rev*. 2011, 91: 1219–1243.
- Hetz C, Russelakis-Carneiro M, Walchli S, Carboni S, Vial-Knecht E, Maundrell K, Castilla J, Soto C. The disulfide isomerase Grp58 is a protective factor against prion neurotoxicity. *J Neurosci* 2005, 25: 2793–802.
- Hetz C. The unfolded protein response: controlling cell fate decisions under ER stress and beyond. *Nat. Rev. Mol. Cell Biol*. 2012, 13: 89–102
- Hirano N, Shibasaki F, Sakai R, Tanaka T, Nishida J, Yazaki Y, Takenawa T, Hirai H. Molecular cloning of the human glucose-regulated protein PDIA3/GRP58, a thiol-dependent reductase. Identification of its secretory form and inducible expression by the oncogenic transformation. *Eur. J. Biochem*. 1995, 234: 336-342.
- Holbrook LM, Sasikumar P, Stanley RG, Simmonds AD, Bicknell AB, Gibbins JM.

- The platelet-surface thiol isomerase enzyme PDIA3 modulates platelet function. *J Thromb Haemost.* 2012, 10(2):278-288.
- Hollien J, Lin JH, Li H, Stevens N, Walter P, Weissman JS. Regulated Ire1-dependent decay of messenger RNAs in mammalian cells. *J Cell Biol.* 2009, 186: 323–331.
- Hollien J, Weissman JS. Decay of endoplasmic reticulum-localized mRNAs during the unfolded protein response. *Science.* 2006, 313: 104–107.
- Holmgren A: Thioredoxin and glutaredoxin systems *J. Biol. Chem.* 1989, 264: 13963-13966.
- Holmgren A: Thioredoxin structure and mechanism: conformational changes on oxidation of the active-site sulfhydryls to a disulphide. *Structure.* 1995, 3: 239-243.
- Holmgren A. Thioredoxin. *Annu Rev Biochem.* 1985, 54: 237-71.
- Holtzman JL. Cellular and animal models for high-throughput screening of therapeutic agents for the treatment of the diseases of the elderly in general and Alzheimer's disease in particular. *Front Pharmacol.* 2013, 4: 59.
- Hui C, Qi X, Qianyong Z, Xiaoli P, Jundong Z, Mantian M. Flavonoids, flavonoid subclasses and breast cancer risk: a meta-analysis of epidemiologic studies. *PLoS One.* 2013, 8(1): e54318.
- Jacquot JP, Rivera-Madrid R, Marinho P, Kollarova M, Le Marechal P, Migniac-Maslow M, Meyer Y. Arabidopsis thaliana NADPH thioredoxin reductase: cDNA characterization and expression of the recombinant protein in Escherichia coli. *J. Mol. Biol.* 1994, 235: 1357-1363.
- Jayasena T, Poljak A, Smythe G, Braidy N, Münch G, Sachdev P. The role of polyphenols in the modulation of sirtuins and other pathways involved in Alzheimer's disease. *Ageing Res Rev.* 2013, 12(4): 867-83.
- Jordan PA, Gibbins JM. Extracellular disulfide exchange and the regulation of cellular function. *Antioxid Redox Signal.* 2006, 8(3-4): 312-24.
- Kaufman RJ, Scheuner D, Schröder M, Shen X, Lee K, Liu CY, Arnold SM. The unfolded protein response in nutrient sensing and differentiation. *Nature Reviews Molecular Cell Biology.* 2002, 3: 411-421.
- Kawahara T, Yanagi H, Yura T, Mori K. Endoplasmic reticulum stress-induced mRNA splicing permits synthesis of transcription factor Hac1p/Ern4p that activates the unfolded protein response. *Mol Biol Cell.* 1997, 8: 1845–1862.
- Kimata Y, Ishiwata-Kimata Y, Ito T, Hirata A, Suzuki T, Oikawa D, Takeuchi M, Kohno K. Two regulatory steps of ER-stress sensor Ire1 involving its cluster formation and interaction with unfolded proteins. *J Cell Biol.* 2007, 179: 75–86.

- Kim-Han JS, O'Malley KL. Cell stress induced by the parkinsonian mimetic, 6-hydroxydopamine, is concurrent with oxidation of the chaperone, PDIA3, and aggresome formation. *Antioxid Redox Signal*. 2007, 9(12): 2255-64.
- Kimmig P, Diaz M, Zheng J, Williams CC, Lang A, Aragón T, Li H, Walter P. The unfolded protein response in fission yeast modulates stability of select mRNAs to maintain protein homeostasis. *eLife*. 2012, 1: e00048.
- Korennykh AV, Egea PF, Korostelev AA, Finer-Moore J, Zhang C, Shokat KM, Stroud RM, Walter P. The unfolded protein response signals through high-order assembly of Ire1. *Nature*. 2009, 457: 687–693.
- Korennykh AV, Korostelev AA, Egea PF, Finer-Moore J, Stroud RM, Zhang C, Shokat KM, Walter P. Structural and functional basis for RNA cleavage by Ire1. *BMC Biol*. 2011, 9:47.
- Kousvelari EE, Banerjee DK, Murty L, Baum BJ. N-linked protein glycosylation in the rat parotid gland during aging. *Mech. Ageing Dev*. 1988, 42: 173–181.
- Kozlov G, Maattanen P, Schrag JD, Pollock S, Cygler M, Nagar B, Thomas DY, Gehring K. Crystal structure of the bb' domains of the protein disulfide isomerase PDIA3. *Structure*. 2006, 14(8):1331-9.
- Lakowicz JR. Principles of Fluorescence Spectroscopy. *Springer*. 2006, 282.
- Lee DY, Lee KS, Lee HJ, Kim DH, Noh YH, Yu K, Jung HY, Lee SH, Lee JY, Youn YC, Jeong Y, Kim DK, Lee WB, Kim SS. Activation of PERK signaling attenuates Abeta-mediated ER stress. *PLoS One*. 2010, 5(5): e10489.
- Lerner AG, Upton J-P, Praveen PVK, Ghosh R, Nakagawa Y, Igarria A, Shen S, Nguyen V, Backes BJ, Heiman M, Heintz N, Greengard P, Hui S, Tang Q, Trusina A, Oakes SA, Papa FR. IRE1 $\alpha$  induces thioredoxin-interacting protein to activate the NLRP3 inflammasome and promote programmed cell death under irremediable ER stress. *Cell Metab*. 2012, 16: 250-264.
- Li H, Korennykh AV, Behrman SL, Walter P. Mammalian endoplasmic reticulum stress sensor IRE1 signals by dynamic clustering. *Proc Natl Acad Sci*. 2010,107(37):16113-8.
- Li Y and Camacho P. Ca<sup>2+</sup>-dependent redox modulation of SERCA 2b by PDIA3. *J. Cell Biol*. 2004, 164: 35-46.
- Lindquist JA, Jensen ON, Mann M, Hämmerling GJ. ER-60, a chaperone with thiol-dependent reductase activity involved in MHC class I assembly. *EMBO J*.1998, 17: 2186-2195.
- Ling Y, Morgan K, Kalsheker N. Amyloid precursor protein (APP) and the biology

- of proteolytic processing: relevance to Alzheimer's disease. *Int. J. Biochem. Cell Biol.* 2003, 35 (11): 1505–1535.
- Lu Y, Liang FX, Wang X. A synthetic biology approach identifies the mammalian UPR RNA ligase RtcB. *Mol Cell.* 2014, 55: 758–770.
- Maattanen, P., Kozlov, G., Gehring, K., Thomas, D. Y. PDIA3 and PDI: multifunctional protein disulfide isomerases with similar domain architectures but differing substrate-partner associations. *Biochem Cell Biol.* 2006, 84(6): 881-9.
- Mahdi AA, Rizvi SH, Parveen A. Role of Endoplasmic Reticulum Stress and Unfolded Protein Responses in Health and Diseases. *Indian J Clin Biochem.* 2016, 31(2): 127-37.
- Manach C, Scalbert A, Morand C, Remesy C, Jimenez L. Polyphenols: food sources and bioavailability. *American Journal of Clinical Nutrition.* 2004, 79: 727–747.
- Mandel SA, Amit T, Weinreb O, Youdim MB. Understanding the broad-spectrum neuroprotective action profile of green tea polyphenols in aging and neurodegenerative diseases. *Journal of Alzheimer's Disease.* 2011, 25: 187–208.
- Marimpietri D, Petretto A, Raffaghello L, Pezzolo A, Gagliani C, Tacchetti C, Mauri P, Melioli G, Pistoia V. Proteome profiling of neuroblastoma-derived exosomes reveal the expression of proteins potentially involved in tumor progression. *PLoS One.* 2013, 8(9): e75054.
- Martin JL, Kenna JG, Martin BM, Thomassen D, Reed GF, Pohl LR. Halothane hepatitis patients have serum antibodies that react with protein disulfide isomerase. *Hepatology.* 1993, 18: 858–63.
- Martin JL. Thioredoxin-a fold for all reasons. *Structure.* 1995; 3(3): 245-50.
- Mishiba K, Nagashima Y, Suzuki E, Hayashi N, Ogata Y, Shimada Y, Koizumi N. Defects in IRE1 enhance cell death and fail to degrade mRNAs encoding secretory pathway proteins in the Arabidopsis unfolded protein response. *Proc Natl Acad Sci.* 2013, 110: 5713–5718.
- Molinari M and Helenius A. Glycoproteins form mixed disulphides with oxidoreductases during folding in living cells. *Nature.* 1999, 402: 90-93.
- Muhlenkamp CR, Gill SS. A glucose-regulated protein, GRP58, is down-regulated in C57B6 mouse liver after diethylhexyl phthalate exposure. *Toxicol Appl Pharmacol.* 1998, 148: 101–8.
- Nemere I, Farach-Carson MC, Rohe B, Sterling TM, Norman AW, Boyan BD, Safford SE. Ribozyme knockdown functionally links a 1,25(OH)2D3 membrane binding protein (1,25D3-MARRS) and phosphate uptake in intestinal cells. *Proc.*

*Natl. Acad. Sci. USA.* 2004, 101: 7392-7397.

Neuhouser ML- Dietary flavonoids and cancer risk: Evidence from human population studies. *Nutr Cancer.* 2004, 50: 1-7.

Nishitoh H, Matsuzawa A, Tobiume K, Saegusa K, Takeda K, Inoue K et al. ASK1 is essential for endoplasmic reticulum stress-induced neuronal cell death triggered by expanded polyglutamine repeats. *Genes Dev.* 2002, 16: 1345-1355.

Obeid M, Tesniere A, Ghiringhelli F, Fimia GM, Apetoh L, Perfettini JL, Castedo M, Mignot G, Panaretakis T, Casares N, M  tievier D, Larochette N, van Endert P, Ciccocanti F, Piacentini M, Zitvogel L, Kroemer G. Calreticulin exposure dictates the immunogenicity of cancer cell death. *Nat Med.* 2007, 13: 54-61.

Oda Y, Okada T, Yoshida H, Kaufman RJ, Nagata K, Mori K. Derlin-2 and Derlin-3 are regulated by the mammalian unfolded protein response and are required for ER-associated degradation. *J. Cell Biol.* 2006, 172: 383-393.

Ohtani H, Wakui H, Ishino T, Komatsuda A, Miura AB. An isoform of protein disulfide isomerase is expressed in the developing acrosome of spermatids during rat spermiogenesis and is transported into the nucleus of mature spermatids and epididymal spermatozoa. *Histochemistry.* 1993, 100: 423-429.

Oikawa D, Tokuda M, Hosoda A, Iwawaki T. Identification of a consensus element recognized and cleaved by IRE1 alpha. *Nucleic Acids Res.* 2010, 38: 6265-6273.

Oliver JD, Roderick HL, Llewellyn DH, High S. PDIA3 functions as a subunit of specific complexes formed with the ER lectins calreticulin and calnexin. *Mol. Biol. Cell.* 1999, 10: 2573-2582.

Oliver JD, van der Wal FJ, Bulleid NJ, High S. Interaction of the thiol-dependent reductase PDIA3 with nascent glycoproteins. *Science.* 1997, 275: 86-88.

Osowski CM, Hara T, O'Sullivan-Murphy B, Kanekura K, Lu S, Hara M, Ishigaki S, Zhu LJ, Hayashi E, Hui ST, Greiner D, Kaufman RJ, Bortell R, Urano F. Thioredoxin-interacting protein mediates ER stress-induced  $\beta$  cell death through initiation of the inflammasome. *Cell Metab.* 2012, 16: 265-273.

Paschen W, Frandsen A. Endoplasmic reticulum dysfunction a common denominator for cell injury in acute and degenerative diseases of the brain? *J Neurochem.* 2001, 79: 719-25.

Pelham HR. Evidence that luminal ER proteins are sorted from secreted proteins in a post-ER compartment. *EMBO J.* 1988, 7(4): 913-8.

P  rez-Jim  nez J, Neveu V, Vos F, Scalbert A. Systematic analysis of the content of 502 polyphenols in 452 foods and beverages: an application of the phenol-explorer database. *J Agric Food Chem.* 2010, 58:4959-4969.

- Prischi F, Nowak PR, Carrara M, Ali MM. Phosphoregulation of Ire1 RNase splicing activity. *Nat Commun.* 2014, 5: 3554.
- Ramírez-Rangel I, Bracho-Valdés I, Vázquez-Macías A, Carretero-Ortega J, Reyes-Cruz G, Vázquez-Prado J. Regulation of mTORC1 complex assembly and signaling by GRp58/PDIA3. *Mol. Cell. Biol.* 2011, 31: 1657-1671.
- Rao RV, Ellerby HM, Bredesen DE. Coupling endoplasmic reticulum stress to the cell death program. *Cell Death Differ.* 2004, 11: 372–80.
- Raturi A and Mutus B. Characterization of redox state and reductase activity of protein disulfide isomerase under different redox environments using a sensitive fluorescent assay. *Free radical biology & medicine.* 2007, 43 (1): 62-70.
- Russell SJ, Ruddock LW, Salo KE, Oliver JD, Roebuck QP, Llewellyn DH, Roderick HL, Koivunen P, Myllyharju J, High S. The primary substrate binding site in the b' domain of PDIA3 is adapted for endoplasmic reticulum lectin association. *J Biol Chem.* 2004, 279(18): 18861-9.
- Rutkowski DT, Arnold SM, Miller CN, Wu J, Li J, Gunnison KM, Mori K, Sadighi Akha AA, Raden D, Kaufman RJ. Adaptation to ER stress is mediated by differential stabilities of pro-survival and pro-apoptotic mRNAs and proteins. *PLoS Biol.* 2006, 4 (11): e374.
- Sadow JJ, Dorstyn L, O'Reilly LA, Tailler M, Kumar S, Strasser A, Ekert PG. ER stress does not cause upregulation and activation of caspase-2 to initiate apoptosis. *Cell Death Differ.* 2014, 21, 475-480.
- Schroder M, Kaufman RJ. ER stress and the unfolded protein response. *Mutat Res.* 2005, 569: 29–63.
- Sciandra F, Angelucci E, Altieri F, Ricci D, Hübner W, Petrucci TC, Giardina B, Brancaccio A, Bozzi M. Dystroglycan is associated to the disulfide isomerase PDIA3. *Exp Cell Res.* 2012, 318(19): 2460-9.
- Sehgal PB. Plasma membrane rafts and chaperones in cytokine/ STAT signaling. *Acta Biochim Pol.* 2003, 50(3): 583-94.
- Seliger B, Wollscheid U, Momburg F, Blankenstein T, Huber C. Characterization of the major histocompatibility complex class I deficiencies in B16 melanoma cells. *Cancer Res.* 2001, 61: 1095–9.
- Shamu CE, Walter P. Oligomerization and phosphorylation of the Ire1p kinase during intracellular signaling from the endoplasmic reticulum to the nucleus. *EMBO J.* 1996, 15: 3028–3039.
- Sidrauski C, Walter P. The transmembrane kinase Ire1p is a site-specific endonuclease that initiates mRNA splicing in the unfolded protein response. *Cell.*

1997, 90: 1031–1039.

So JS, Hur KY, Tarrío M, Ruda V, Frank-Kamenetsky M, Fitzgerald K, Koteliansky V, Lichtman AH, Iwawaki T, Glimcher LH, Lee AH. Silencing of lipid metabolism genes through IRE1 $\alpha$ -mediated mRNA decay lowers plasma lipids in mice. *Cell Metab.* 2012, 16: 487–499.

Song JI, Grandis JR. STAT signaling in head and neck cancer. *Oncogene.* 2000, 19: 2489-2495.

Štefanková P, Kollárová M and I. Barák. Thioredoxin – Structural and Functional Complexity. *Gen. Physiol. Biophys.* 2005, 24: 3-11.

Sun Y, Zhang H, Sun Y, Zhang Y, Liu H, Cheng J, Bi S, Zhang H. Study of interaction between protein and main active components in *Citrus aurantium* L. by optical spectroscopy. *Journal of Luminescence.* 2010, 130 (2): 270-279.

Tirasophon W, Lee K, Callaghan B, Welihinda A, Kaufman RJ. The endoribonuclease activity of mammalian IRE1 autoregulates its mRNA and is required for the unfolded protein response. *Genes Dev.* 2000, 14(21): 2725-36.

Tohda C, Urano T, Umezaki M, Nemere I, Kuboyama T. Diosgenin is an exogenous activator of 1,25D3-MARRS/Pdia3/PDIA3 and improves Alzheimer's disease pathologies in 5XFAD mice. *Sci Rep.* 2012, 2: 535.

Tourkova IL, Shurin GV, Chatta GS, Perez L, Finke J, Whiteside TL, Ferrone S, Shurin MR.. Restoration by IL-15 of MHC class I antigen-processing machinery in human dendritic cells inhibited by tumor-derived gangliosides. *J Immunol* 2005, 175: 3045–52.

Trnkova L, Ricci D, Grillo C, Colotti G, Altieri F. Green tea catechins can bind and modify PDIA3/PDIA3 activity. *Biochim Biophys Acta.* 2013, 1830(3): 2671-82.

Turano C, Coppari S, Altieri F, Ferraro A. Proteins of the PDI family: unpredicted non-ER locations and functions. *J Cell Physiol.* 2002, 193(2): 154-63.

Upton J-P, Wang L, Han D, Wang ES, Huskey NE, Lim L, Truitt M, McManus MT, Ruggero D, Goga A, Papa FR, Oakes SA. IRE1 $\alpha$  cleaves select microRNAs during ER stress to derepress translation of proapoptotic caspase-2. *Science.* 2012, 338: 818-822.

Urano F, Wang X, Bertolotti A, Zhang Y, Chung P, Harding HP et al. Coupling of stress in the ER to activation of JNK protein kinases by transmembrane protein kinase IRE1. *Science.* 2000, 287: 664–666.

Vauzour D, Rodriguez-Mateos A, Corona G, Oruna-Concha MJ, Spencer JP. Polyphenols and human health: prevention of disease and mechanisms of action.

*Nutrients*. 2010, 2(11): 1106-31.

Wiseman RL, Zhang Y, Lee KP, Harding HP, Haynes CM, Price J, Sicheri F, Ron D. Flavonol activation defines an unanticipated ligand-binding site in the kinase-RNase domain of IRE1. *Mol Cell*. 2010, 38(2): 291-304.

Woo HD and Kim J. Dietary Flavonoid Intake and Smoking-Related Cancer Risk: A Meta-Analysis. *Plos One*. 2013 Sep 19; 8(9): e75604.

Wu W, Beilhartz G, Roy Y, Richard CL, Curtin M, Brown L, Cadieux D, Coppolino M, Farach-Carson MC, Nemere I, Meckling KA. Nuclear translocation of the 1,25D3-MARRS (membrane associated rapid response to steroids) receptor protein and NFkappaB in differentiating NB4 leukemia cells. *Exp. Cell Res*. 2010, 316: 1101-1108.

Wu Y, Ahmad SS, Zhou J, Wang L, Cully MP, Essex DW. The disulfide isomerase PDIA3 mediates platelet aggregation, hemostasis, and thrombosis. *Blood*. 2012, 119(7):1737-1746.

Yoshida, H., Matsui, T., Hosokawa, N., Kaufman, R. J., Nagata, K. and Mori, K. A time-dependent phase shift in the mammalian unfolded protein response. *Dev. Cell*. 2003, 4: 265-271.

Yu H, Jove R. The STATs of cancer-new molecular targets come of age. *Nature reviews. Cancer*. 2004, 4: 97-105.

Yu H, Pardoll D, Jove R. STATs in cancer inflammation and immunity: a leading role for STAT3. *Nature reviews. Cancer*. 2009, 9: 798-809.

Zhang K, Wong HN, Song B, Miller CN, Scheuner D, Kaufman RJ. The unfolded protein response sensor IRE1 $\alpha$  is required at 2 distinct steps in B cell lymphopoiesis. *J. Clin. Invest*. 2005, 115: 268–281.

Zhou J, Liu CY, Back SH, Clark RL, Peisach D, Xu Z, Kaufman RJ. The crystal structure of human IRE1 luminal domain reveals a conserved dimerization interface required for activation of the unfolded protein response. *Proc Natl Acad Sci USA*. 2006, 103(39): 14343-8.